Cement and Concrete Research 174 (2023) 107339

Contents lists available at ScienceDirect

Cement and Concrete Research

journal homepage: www.elsevier.com/locate/cemconres

Influence of temperature on phase assemblages of belite-ye'elimite cement

Natechanok Chitvoranund [a,*,1], Barbara Lothenbach [b], Diana Londono-Zuluaga [a,2], Frank Winnefeld [b], Karen Scrivener [a]

[a] Laboratory of Construction Materials, LMC, EPFL-STI-IMX, Station 12, CH-1015 Lausanne, Switzerland
[b] Laboratory for Concrete & Asphalt, Swiss Federal Laboratories for Materials Science and Technology, Empa, Dübendorf, Switzerland

ARTICLE INFO

Keywords:
Belite-ye'elimite cement
Hydration
Phase assemblages
Thermodynamic modelling
Temperature

ABSTRACT

This paper studies the effect of temperature on the phase assemblages of belite-ye'elimite cement. A comparison is made between thermodynamic modelling and experimental data at 28 and 180 days of hydration at 5, 20, 40, and 60 °C. The fast reaction of ye'elimite and anhydrite resulted in the formation of ettringite, monosulfate and $Al(OH)_3$ during the first day. The slow reaction of belite led to important changes in phase assemblages. The formation of C-S-H was predicted and observed at high belite degree of reaction. Siliceous hydrogarnet was observed experimentally only at 60 °C. The strätlingite content decreased at elevated temperatures. C-S-H and strätlingite were observed to be finely intermixed with the AFm phases. The belite reaction contributes to additional strength after 28 days of hydration. The relationships between the compressive strength and bound water or calculated porosity were found but the effect of temperature is still unclear.

1. Introduction

Calcium sulfoaluminate cement (CSA) is used as an alternative binder with lower CO_2 emissions than Portland cement (PC) [1] as it contains less limestone and has a lower sintering temperature [2]. CSA is a general term for binders containing ye'elimite ($C_4A_3\overline{S}$, $4CaO{\cdot}3Al_2O_3{\cdot}SO_3$). CSA cement contains more alumina than PC and they can be classified into two main groups: (i) high ye'elimite CSA and (ii) low ye'elimite CSA, also called BYF (Belite-Ye'elimite-Ferrite). The different clinker composition changes the hydrated phase assemblages, leading to different properties of the concrete made from these binders [3–5].

Even though the hydration of BYF cement has been widely studied, most studies have been carried out at room temperature. The relevant hydration reactions of a BYF system can be described in the following, idealized way: The reaction of ye'elimite and calcium sulfate with water occurs fast, resulting in the formation of ettringite and aluminium hydroxide (AH_3) gel during the first hours. After sulfate depletion monosulfate $[Ca_4Al_2(OH)_{12}]^{2+}[SO_4{\cdot}nH_2O]^{2-}$, the AFm-type phase and AH_3 form. Ettringite and AFm are crystalline, while AH_3 is generally present as an amorphous or nanocrystalline phase in this type of cement [6–8]. CAH_{10} can be formed as a metastable phase when the molar ratio of calcium sulfate/ye'elimite is low [9,10]. Belite reacts at later ages, forming strätlingite (C_2ASH_8, $[Ca_4Al_2(OH)_{12}]^{2+}[(AlSi(OH)_8)_2{\cdot}nH_2O]^{2-}$), another AFm-type phase [7,11,12], and calcium silicate hydrates (C-S-H). In addition, sometimes, siliceous-hydrogarnet can be observed at late ages due to the reaction of ferrite [11,13].

The reactivity of BYF cements depends on many factors such as the amount and reactivity of calcium sulfate [12,14], amount of mixing water [11], and the presence and amount of minor phases, in particular mayenite [15]. The hydration of BYF may also be influenced by temperature, which affects not only the hydration kinetics, but also the types of hydrates formed [16–18]. It has been claimed that at higher temperatures ettringite can be transformed to monosulfate and $CaSO_4$ due to the increase of ettringite solubility with temperature, while the stability of monosulfate varies little with temperature [19,20]. Kaufmann et al. [17], however, showed that ettringite can be stable up to 90 °C in ye'elimite-rich cement. The kind of aluminium hydroxide (AH_3) formation also depends on temperature. Amorphous or nanocrystalline AH_3 is formed at temperatures below 60 °C. The AH_3 crystallinity increases with temperature and gibbsite has been reported to form above 60 °C [20].

The phases formed during hydration evolve with time. For example, once belite starts to react, $Al(OH)_3$, may be consumed by the formation

* Corresponding author.
E-mail address: natechanok.chitvoranund@ri.se (N. Chitvoranund).
[1] Current address: Materialdesign Unit, Department of Infrastructure and Concrete Technology, Research Institute of Sweden (RISE), Borås, Sweden.
[2] Current address: Research and Quality Centre, Cementir Holding S.p.A., Aalborg, Denmark.

https://doi.org/10.1016/j.cemconres.2023.107339
Received 22 May 2023; Received in revised form 10 September 2023; Accepted 28 September 2023
Available online 11 October 2023

Table 1
Chemical composition, mineralogy and distribution value of the raw material.

PSD (μm)	BY clinker	Mayenite	Anhydrite	XRD (wt.-%)	BY clinker	Mayenite	Anhydrite
$D_{v,10}$*	0.54	2.77	0.25	β-C_2S	60.3	–	–
$D_{v,50}$*	4.34	8.49	8.97	C_3A	–	1.9	–
$D_{v,90}$*	15.88	30.14	31.75	$C_4A_3\overline{S}$***	39.4	–	–
XRF (wt%)				CA	–	0.6	–
SiO_2	18.9	0.1	2.5	$C_{12}A_7$	–	97.5	–
Al_2O_3	20.9	50.1	0.6	Dolomite	–	–	6.9
Fe_2O_3	0.0	0.1	0.3	Portlandite	–	–	0.1
CaO	53.2	47.6	38.7	Gypsum	–	–	2.5
MgO	0.1	–	1.9	Free Lime	0.3	–	–
SO_3	6.3	0.1	52.2	Anhydrite	–	–	77.7
K_2O	–	–	0.2	Quartz	–	–	2.3
Na_2O	0.1	0.1	0.1	Rutile	–	–	1.2
Others	0.0	0.0	0.2	Muscovite	–	–	8.5
LOI**	0.6	1.2	3.4	Cristobalite	–	–	0.7
SUM	100.1	99.4	100.2	SUM	100.0	100.0	99.9

* D_v = the volume moment mean diameter.
** LOI = Loss on ignition.
*** $C_4A_3\overline{S}$ = both orthorhombic and cubic polymorphs.

of strätlingite and C-A-S-H [11]. These changes during hydration and their effect on the microstructure are poorly understood as particularly strätlingite, C-S-H and non/nano-crystalline $Al(OH)_3$ are difficult to observe and quantify in low quantities due to their poorly crystalline nature [21]. Thermodynamic modelling can be used as a tool to predict the phase assemblages at equilibrium [6,7,21–23]. It can also be used to predict the changes occurring during hydration if the degree of reaction of the starting phases is well-characterized [17,23].

This work compares the thermodynamic modelling of mature phase assemblages in CSA-belite cements at different temperatures with experimental observations, including in-depth analysis of the microstructure observed by various techniques. The output of this analysis is the identification of knowledge gaps that should be the focus of future investication. A simplified system based on a laboratory belite-ye'elimite (BY) clinker with calcium sulfate was used. The hydration and compressive strength of this BY cement was investigated from 5 to 60 °C. The hydrated cements were characterized in detail by XRD, TGA, SEM-EDS mapping and image analysis. The pore solutions were analysed by ion chromatography (IC).

2. Materials and methods

2.1. Raw materials and mixture design

The initial goal was to synthesize β-belite and ye'elimite separately. However, belite synthesis could not be reproduced on a large scale due to high γ-belite content which is not reactive. Therefore, a polyphase clinker of belite-ye'elimite clinker was used in this study because it was easier to synthesize in large quantities.

Laboratory prepared belite-ye'elimite clinker, mayenite and a natural anhydrite source were used. The belite-ye'elimite clinker was prepared using an adaptation of the cylinder method presented by Li et al. [24]. Chemical reagents (calcium carbonate, nano silica, calcium sulfate dihydrate and aluminium oxide) were ground for 24 h with water. Then, the mix was poured in cylinders and dried for at least 48 h at 105 °C. Afterwards, the cylinders were heated to 1300 °C in a laboratory furnace, at a heating rate of 7 °C/min, maintained at the maximum temperature for one hour, and then rapidly air-cooled to room temperature. Mayenite ($C_{12}A_7$) was synthesized following the steps in [15]. The laboratory prepared BY clinker was blended with ground anhydrite from a natural source. Anhydrite was added to obtain a calcium sulfate to ye'elimite molar ratio of 1:1. The pure BY cement had a long setting time around one day at 20 °C, therefore a small amount of mayenite was added to accelerate the ye'elimite reaction and bring it into the normal range found in commercial cement [15]. The system contained 89.3 % of BY clinker, 10.6 % of anhydrite, 0.25 % of mayenite with a total content of 52.3 % C_2S and 36.9 % ye'elimite.

2.2. Raw materials characterization

The chemical composition, mineralogy and particle size distribution of the raw materials were characterized by X-ray fluorescence (XRF), quantitative X-ray powder diffraction (XRD) and laser diffraction (Malvern MasterSizer S) as shown in Table 1.

The BY clinker was ground for 60 s in a concentric disc mill in batches of 100 g with 7–10 drops of isopropanol as a grinding aid. The samples were characterized in a X'Pert Pro PANalytical diffractometer in Bragg-Brentano mode, using a CuK_α source at 45 kV and 40 mA. Continuous spinning was applied during the data acquisition. Samples were scanned between 5 and 70 degrees (2 theta) for 30 min. The mineralogy of raw materials was determined by the Rietveld method using PANalytical Highscore Plus 4.8 software. The manual background was manually fit with base points. The refinement was carried out on specimen displacement, scale factor, and preferred orientation. β-belite was quantified and no -belite was observed. The value of ye'elimite ($C_4A_3\overline{S}$) reported in Table 1 is combined with the two polymorphs which the average content of orthorhombic is 34 wt% and cubic is 6 wt%.

Particle size distributions were measured by laser diffraction using a MalvernSizer S. The powder, approximately 0.1 g, was suspended in isopropanol. The suspension was stirred and placed in an ultrasonic probe for 15 min. Then, the suspension was transferred to the measuring unit previously filled with isopropanol, until the proper level of obscuration was reached.

2.3. Preparation of cement pastes

The binders and deionized water were equilibrated overnight at the intended curing temperature before mixing. The dry powders were blended with an overhead lab mixer for 1 min at 500 rpm. Cement pastes were prepared with a water to binder ratio (w/b) of 0.6 at 1600 rpm in a batch of 240 g of dry powder for 2 min. The samples were cast into 50 ml polypropylene containers and sealed with a few drops of distilled water on top of the paste to keep it saturated during curing. The samples were stored up to 1 year at 5, 20, 40 and 60 °C with a variation less than ±1 °C. The samples were analysed by X-ray diffraction (XRD), thermogravimetric analysis (TGA), scanning electron microscopy and energy dispersive X-ray spectroscopy (SEM-EDX). For the pore solution experiments, additional larger samples were cast in 500 ml

Table 2
Mineralogical references for quantitative Rietveld refinement on XRD patterns (ICSD).

Phase	ICSD	Ref	Phase	ICSD	Ref
Belite	81096	Mumme et al. 1995 [28]	CAH_{10}	407150	Guirado et al. 1998 [29]
Ye'elimite (orthorhombic)	80361	Calos et al. 1995 [30]	Gibbsite (AH_3)	6162	Saalfeld and Wedde 1974 [31]
Ye'elimite (cubic)	9560	Saalfeld and Depmeier 1972 [32]	Strätlingite	69413	Rinaldi et al. 1990 [33]
Mayenite	261586	Ponomarev et al. 1970 [34]	Ettringite	155395	Goetz-Neunhoeffer and Neubauer 2006 [35]
Gypsum	409581	Boeyens and Ichharam 2002 [36]	Monosulfate-12	100138	Allmann 1977 [27]
Anhydrite	28546	Höhne 1963 [37]	Monosulfate-14	100138	Allmann 1977 [27]
Dolomite	66333	Ross and Reeder 1992 [38]	Si-Katoite	1720177	Ferro et al. 2003 [39]
			CSH crystalline	1028762	Richardson 2014 [40]

polypropylene containers and stored at different temperatures.

2.4. Methods

2.4.1. XRD

The cement pastes were cut with a circular saw with water-cooling. Fresh slices (without drying) of 2–3 mm thickness were gently polished with sandpaper to remove the suface that mostly in contact with water. The preparation does not take >5 min. Then, the samples were analysed with a PANalytical X'per Pro diffractometer using $CuK_{\alpha1\alpha2}$ source (45 kV, 40 mA) in the Bragg-Brentano configuration (fixed divergent slit of 1/2°, a Soller slit of 0.04 rad and mask of 15 mm). The patterns were recorded between 5 and 70° (2 theta) using a step size of 0.017° for a total duration of 14 min. Rutile (Kronos® 2220 97 wt% crystalline composition and average particle size of 400 nm) was used as an external standard to quantify the amorphous content [25,26]. The phase assemblage was quantified by the Rietveld refinement method using PANalytical Highscore Plus 4.8 software with the reference pattern presented in Table 2. The quantification of XRD result is normalized to 100 g of dry binder. The refinement method was carried out similarly to the raw materials analysis. The amount of Ms_{14} was quantified by using the kuzelite crystal structure (ICSD-100138) [27] with refined lattice parameters of a ~ 5.75 ± 0.01 Å and c ~ 28.63 ± 0.01 Å for all temperatures except at 60 °C (c ~ 28.53 Å). The degree of hydration (DoH) of anhydrous phases at time t was calculated from the mass fraction reacted to the initial amount. The formula for the calculation is shown in Eq. (2-1). Two replicates were analysed indicating the error in XRD quantification is around 2 wt%.

$$\mathrm{DoH}\ (\%)_t = \left(\frac{W_0 - W_t}{W_0}\right) \times 100 \tag{2-1}$$

where W_0 is the initial amount, W_t is the amount at time t.

A section of the XRD patterns between 5 and 30° 2theta is shown in Appendix A.

2.4.2. TGA

The hydration of the cement pastes was stopped by solvent exchange using isopropanol [41]. The sample slices were immersed in isopropanol for one week. The isopropanol was changed at 1, 3 and 7 days. The samples were dried in a desiccator under light vacuum for at least 7 days before the analysis. A small piece of the sample was ground on all sides to remove any carbonated material before being gently crushed in a ceramic mortar. 50 mg of sample powder was placed in a 150 µl alumina crucible with a lid, then was analysed by TGA (Mettler Toledo TGA/SDTA 851) from 30 to 1000 °C with a heating rate of 10 K/min under 30 ml/min N_2 gas flow. The weight loss from TGA analysis was used to obtain the amount of chemical bound water (BW) as shown in Eq. (2-2). Then, the amount of bound water was normalized to 100 g of dry binder.

$$\mathrm{BW} = \frac{W_{40} - W_{550}}{W_{550}} \tag{2-2}$$

where W_t is the dry sample weight in grams at the respective temperature (°C). The amount of free water was calculated from the difference between the mixing water and the bound water (BW) determined by TGA.

2.4.3. SEM-EDS

The same method of stopping hydration as for TGA analysis was applied to samples for SEM-EDX. A piece of the sample was gently ground with a silicon carbide paper of 1200 grit to smooth the surface. The samples were embedded in a low-viscosity epoxy resin under vacuum. The impregnated samples were hand-ground on a SiC paper of 1200 grit with isopropanol as a lubricant until the sample surface was uncovered. The polished samples were stored in a vacuum desiccator for at least two days to evaporate the isopropanol before coating it with carbon. Full detail of the method is given in [41]. A polished section was analysed in a GeminiSEM 300 under high vacuum mode for the high-resolution BSE images (field emission) and using an FEI Quanta 200 scanning electron microscope equipped with a Bruker ASX microanalysis XFlash 4030 silicon drift detector for the EDS mapping (tungsten filament). The accelerating voltage was 12 kV in both instruments, with a working distance of 8.5 mm for BSE image acquisition, and 12.5 mm for EDS mapping.

2.4.4. Image analysis

Image analysis was carried out to identify the formation of phases of interest in the microstructure. The BSE images and EDS mapping data were linked using the edxia software [42]. The ratio plots of Si/Ca – Al/Ca and Al/Ca – S/Ca from EDS maps provide the composition of the main phases present in the sample. Using the graphical interface of edxia, manually selected points in the ratio plots are mapped onto the BSE image to identify areas with the selected composition.

2.4.5. Pore solution analysis

The pore solutions of the hardened samples were extracted by the steel die method [43] using pressure up to 250 N/mm^2. The solutions were filtered immediately with nylon filters (0.45°µm). The hydroxide concentrations of the pore solutions were calculated from pH measurements with a pH electrode, calibrated against KOH solutions with known concentrations [44]. The concentrations of Na, K, Ca, Si, S, Al and Cl were determined by ion chromatography (Dionex DP ICS-3000). Each sample was diluted by a factor of 10, 100 or 1000 before measurement depending on the ion concentration; standards from 0.1 to 50 mg/l were used for calibration. The relative error of the measurements was about 10 %.

2.4.6. Thermodynamic modelling

Thermodynamic modelling was carried out using GEMS-PSI software [45,46] with the PSI-Nagra database [47] and the cement CEMDATA18 database [20]. The mean degree of hydration from Rietveld quantification of the main clinker phases at 28 days and at 180 days of hydration was used as an input for the calculations. Some minor phases in the natural anhydrite (quartz, muscovite, cristobalite and rutile) were

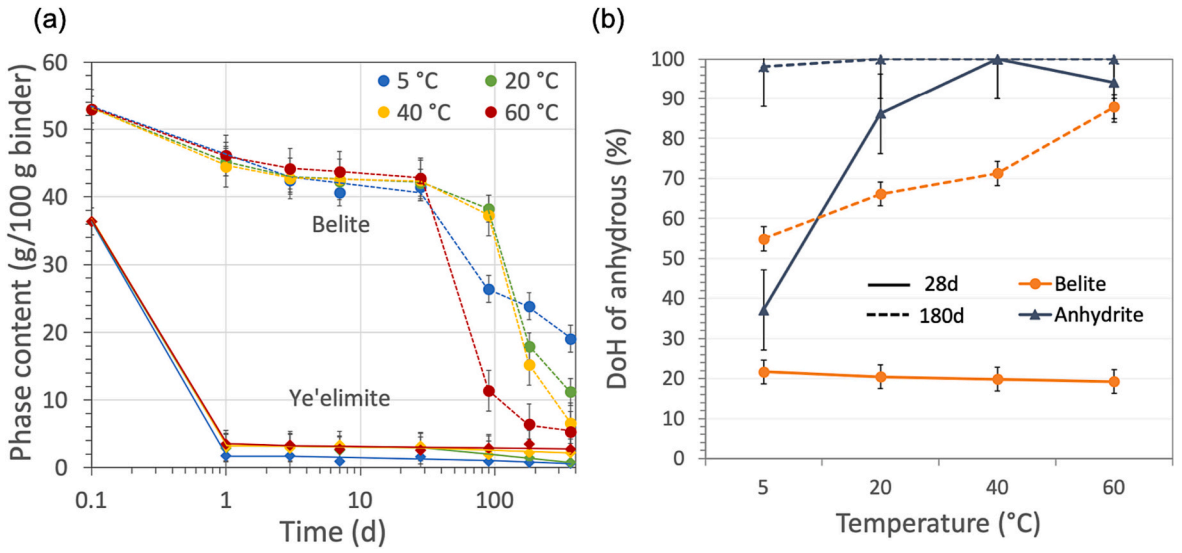

Fig. 1. (a) Phase content of anhydrous phases in BY cement paste up to 365 days of hydration (b) Degree of hydration (DoH) of belite and anhydrite at 28 days and 180 days of hydration obtained by XRD with Rietveld refinement.

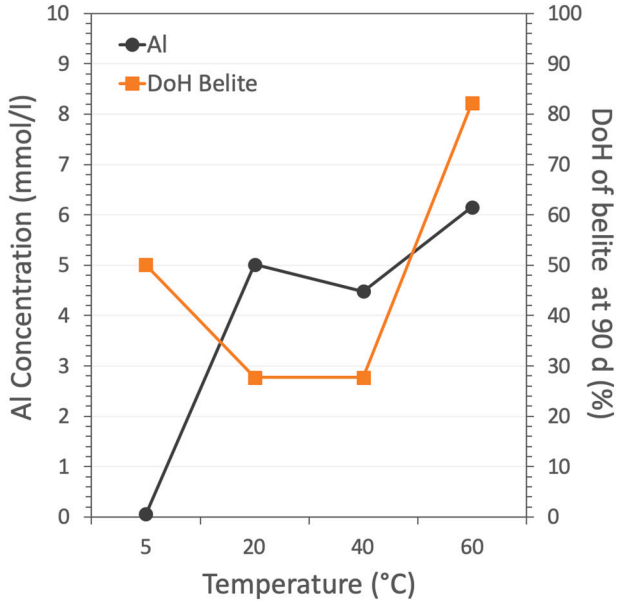

Fig. 2. The concentration of Al in the pore solution of the BY system and belite reaction degree at 90 days for samples cured at 5, 20, 40 and 60 °C.

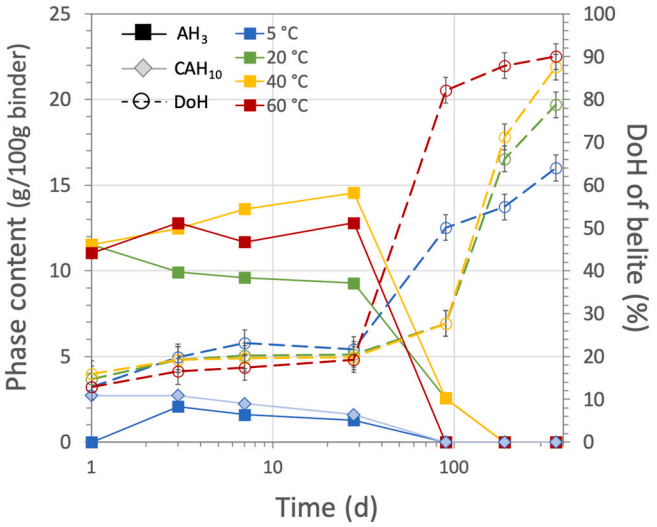

Fig. 3. Relation between the formation of CAH_{10} at 5 °C and/or AH_3 at 20–60 °C and the degree of hydration of belite in the BY system as a function of time.

considered as inert phases during the calculations. The Al-incorporation in C-S-H is not considered as there was little C-S-H and thus Al uptake could not be measured accurately. Therefore, CSHQ from CEMDATA18 was used without modification. The formation of microcrystalline Al $(OH)_3$ was considered at 5, 20 and 40 °C, and of gibbsite at 60 °C [20]. In line with the experimental observations, the formation of Al-containing siliceous hydrogarnet was only allowed at 60 °C at 180 days.

2.4.7. Mortar compressive strength

The samples were prepared following the EN196–1 standard except for the water to binder ratio (w/b) was set to 0.6, as for the cement paste samples. The homogenized dry binders and the deionized water were equilibrated overnight at the intended curing temperature before mixing. The mixing was carried out at room temperature. The standardized sand was used in the sand to binder ratio (S/B) of 3 by mass. The mortar samples were placed in the boxes and cured at 5, 20, 40 and 60 °C until the time of testing from 1 up to 365 days.

Table 3
Average degree of hydration (DoH) at 28 days and 180 days of anhydrous phases.

% DoH	28d	180d
Belite	20.5	70.0
Ye'elimite	93.0	94.5
Anhydrite	82.0	99.5

3. Results and discussion

3.1. Reaction of belite and ye'elimite in BY cement paste from experimental data

The unreacted amount of belite and ye'elimite in the BY cement paste from 1 up to 365 days is shown in Fig. 1a. Ye'elimite reacts very

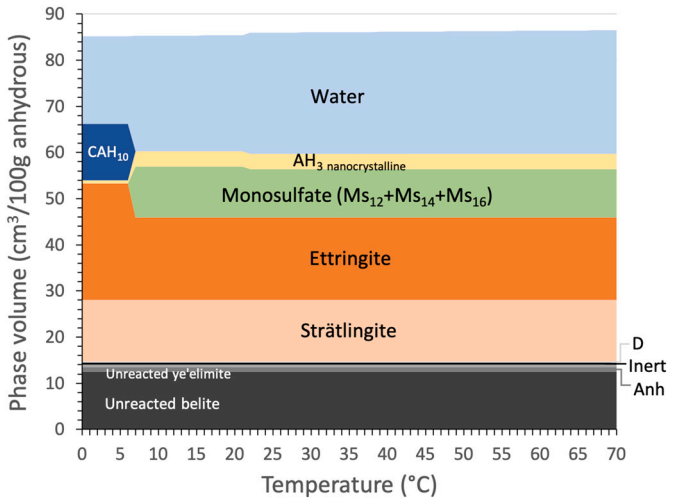

Fig. 4. Calculated volume of solids in a hydrated BY cement with low belite reaction as a function of temperature using the average DoH values at 28 days at different temperatures: D = dolomite and Anh = anhydrite.

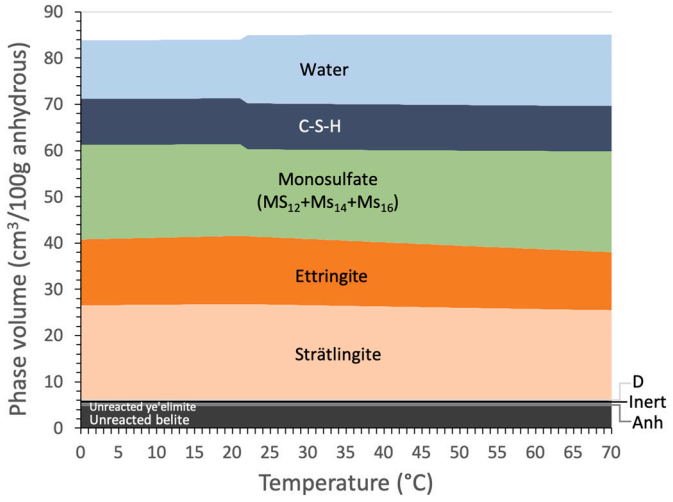

Fig. 5. Calculated volume of solids in the hydrated BY cement of low belite reaction as a function of temperature using the average DoH values at 180 days at different temperatures: D = dolomite and Anh = anhydrite.

quickly and nearly complete (>90 %) during the first day; changes are negligible between 1 and 365 days. The consumption of ye'elimite at 5 °C is slightly higher than at the other curing temperatures. For belite, a slow reaction is observed with no significant difference between the different curing temperatures during the first 28 days. However, after 90 days more belite is consumed at 60 °C compared to the other temperatures, followed by 5 °C, while there is a little reaction at 20 and 40 °C. Currently, there is no clear explanation why belite is more reactive at 5 °C than at 20 and 40 °C. At 180 days, the reaction of belite is dramatically increased at 20 and 40 °C from 90 days, whereas it is slightly increased at 5 and 60 °C. The 28 days and 180 days can be considered as two extreme cases: low belite reaction (28 days of hydration) and high belite reaction (180 days of hydration). From Fig. 1b, belite shows a similar DoH of about 20 % at 28 days at all temperatures. At 180 days, the DoH of belite increases as a function of temperature between 50 and 90 %. Anhydrite shows high DoH of >80 % at 20 °C and above and is almost fully reacted at 40 °C and above after 28 days. Low anhydrite reaction was observed on the sample cured at 5 °C at 28 days, but nearly all was consumed at 180 days.

It has been reported that the presence of aluminium concentrations

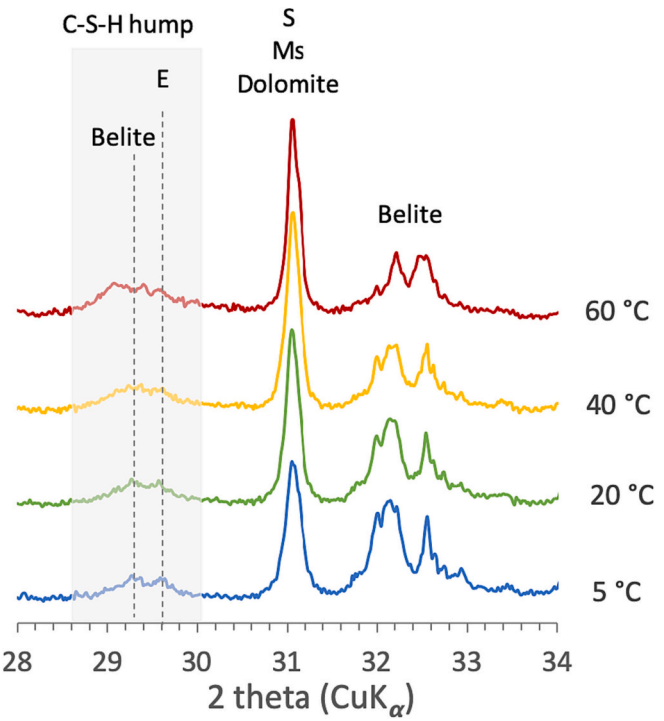

Fig. 6. C-S-H hump at different temperatures at the zoomed section of XRD patterns between 2theta 28–34° of 180 days sample: C-S-H = calcium silicate hydrates, E = ettringite, S = strätlingite, Ms = monosulfate.

(in the millimolar range) in the pore solution may slow down the dissolution of the alite considerably [48,49]. The Al concentration in the pore solution at 90 days is shown in Fig. 2 and summarized with the complete solution composition after 90 days in Appendix B. There is no consistent relation between the concentration of Al in the solution and the degree of belite reaction: the DoH of belite was the highest at 60 °C where the Al concentration in solution was also the highest. However, we also observed a higher degree of belite reaction at 5 °C at very low Al concentrations, indicating that not only the Al concentration but also the temperature and probably other factors affect the belite reaction in the studied system. The belite reaction might also be related to the undersaturation with respect to belite in the pore solution [48] However, no clear relation could be found between belite reaction and undersaturation (see saturation indices in Appendix B) based on the very limited solution data available in our study.

Fig. 3 shows that when belite starts to react, AH_3 and CAH_{10} disappear to form strätlingite. Thermodynamic modelling in the following section supports the idea that this is a consequence rather than a cause of the belite reaction, as discussed in detail there.

3.2. *Thermodynamic modelling of the effect of temperature and effect of belite reaction on phase assemblages*

Thermodynamic modelling was used to simulate the impact of temperature for the low belite reaction (at 28 days) and high reaction (at 180 days). An average value of DoH from the experimental data at the different temperatures (Table 3) was taken as an input to simplify the thermodynamic modelling calculation and to see the effect of temperature (between 0 and 70 °C) on the phase assemblage.

3.2.1. *Effect of temperature at low belite reaction degree*

Fig. 4 shows the effect of temperature on the phase assemblages with low belite reaction (20 % DoH; 28 days) in terms of the volume of solids. Thermodynamic modelling indicates that at all temperatures ettringite, strätlingite and aluminium hydroxide (AH_3) are expected to be the main

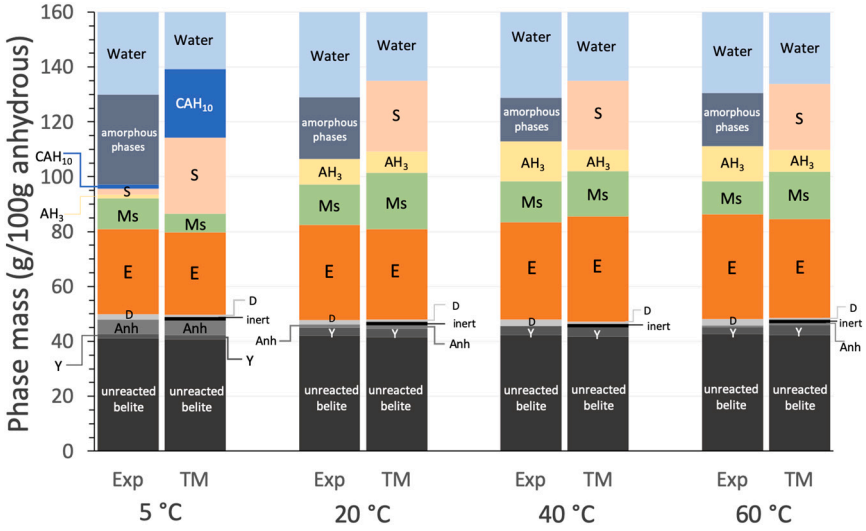

Fig. 7. Comparison of phase assemblages at different temperatures between thermodynamic modelling and the experimental data at 28 days: Y = ye'elimite, Anh = anhydrite, D = dolomite, E = ettringite, Ms = total monosulfate, S = strätlingite, and C-S-H = calcium silicate hydrates.

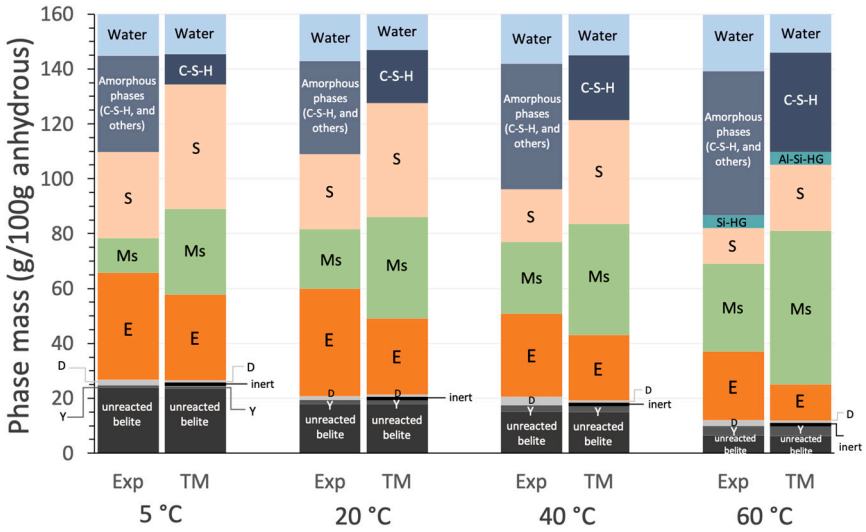

Fig. 8. Comparison of phase assemblages at different temperatures between thermodynamic modelling and the experimental data at 180 days: Y = ye'elimite, D = dolomite, E = ettringite, Ms = total monosulfate, S = strätlingite, Si-HG = siliceous hydrogarnet, Al-Si-HG = Al-containing siliceous hydrogarnet and C-S-H = calcium silicate hydrates (observed in Section 3.5.2).

hydrate phases. The only change is at around 7 °C. Below 7 °C, ettringite and CAH_{10} are predicted to form. At temperatures above 7 °C, CAH_{10} is no longer stable, and monosulfate is present together with nano-crystalline AH_3. This results in a significant decrease in the total volume of solid. The temperature at which CAH_{10} disappears depends on the solubility of the AH_3. CAH_{10} might be stable up to 30 °C in the presence of amorphous $Al(OH)_3$ and in the absence of portlandite or C-S-H, due to high solubility of amorphous $Al(OH)_3$ [50], which is formed at early stages of hydration. With time, as $Al(OH)_3$ recrystallizes to microcrystalline $Al(OH)_3$ and to gibbsite in the longterm, its solubility decreases, leading to a destabilisation of CAH_{10} at low temperature [50]. At temperatures above 7 °C little further change is predicted; the small step in the water and monosulfate amount around 20 °C is due to the change of the hydration state of monosulfate from 16 to 14 stoichiometric molecules of H_2O in its structure at this temperature [51]. No significant change in the amount of strätlingite is seen and ettringite is stable up to at least 70 °C (maximum temperature studied) in agreement with the observations on CSA cements [17].

3.2.2. *Effect of temperature at high belite reaction degree*

The effect of temperature on the phase assemblages with high belite reaction is shown in Fig. 5. Ettringite, monosulfate, strätlingite and C-S-H are predicted to form at all temperatures. The higher availability of CaO at high belite reaction of 70 %, means that CAH_{10} and AH_3 are not predicted to form, while more strätlingite and C-S-H are formed instead. Also, more monosulfate and less ettringite are predicted compared to the low belite case.

For the high belite reaction case, the temperature has little effect on the hydrates expected to be present, only the amount of ettringite decreases slightly above 20 °C, whereas more monosulfate is expected to be present with increasing temperature. Also, strätlingite is slightly decreased at higher temperature, while slightly more C-S-H should form. Fig. 5 illustrates that the volume of solid in the hydrated CSA remains quite similar from 0 to 20 °C. Again, the small step of the solid volume at 20 °C corresponds to the decrease of stoichiometric water in monosulfate.

From Figs. 4 and 5, it is obvious that temperature has little effect on the expected hydrates at a constant reaction degree of belite. For low

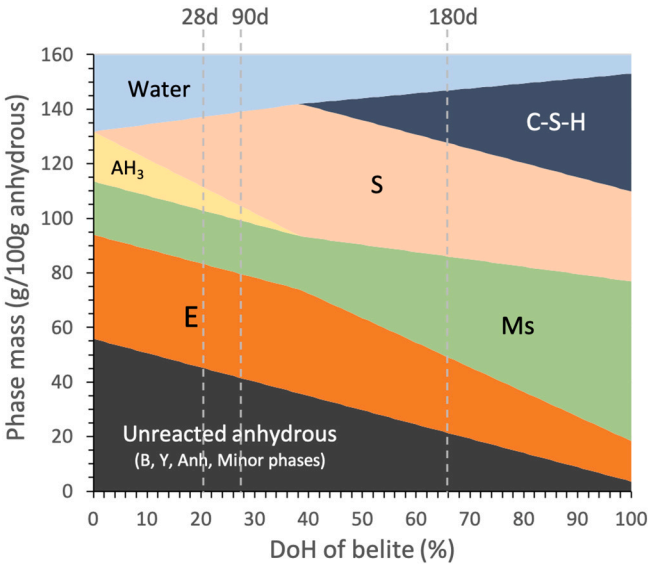

Fig. 9. Phase assemblages in mass as a function of DoH of belite (using the data at 20 °C as an input) calculated by thermodynamic modelling at 20 °C: B = belite, Y = ye'elimite, Anh = anhydrite, E = ettringite, Ms = total monosulfate, S = strätlingite, and C-S-H = calcium silicate hydrates.

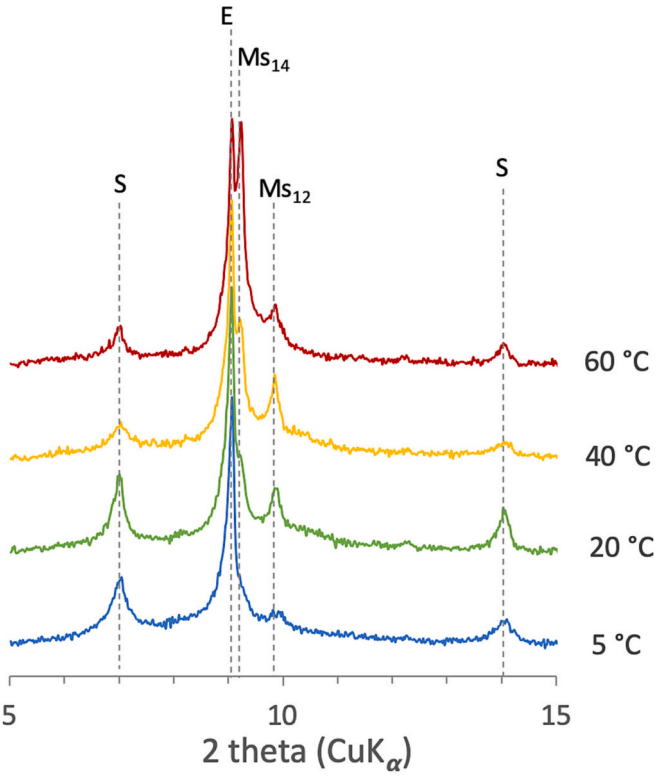

Fig. 10. Main hydration products at all curing temperatures after 180 days at a zoomed section of XRD patterns between 2theta 5–15°: E = Ettringite, Ms = monosulfate and S = strätlingite.

belite reaction, increasing temperature leads to disappearance of CAH_{10} at around 7 °C. At high belite reaction, no significant change of phase assemblage is calculated but only small differences in the relative quantities.

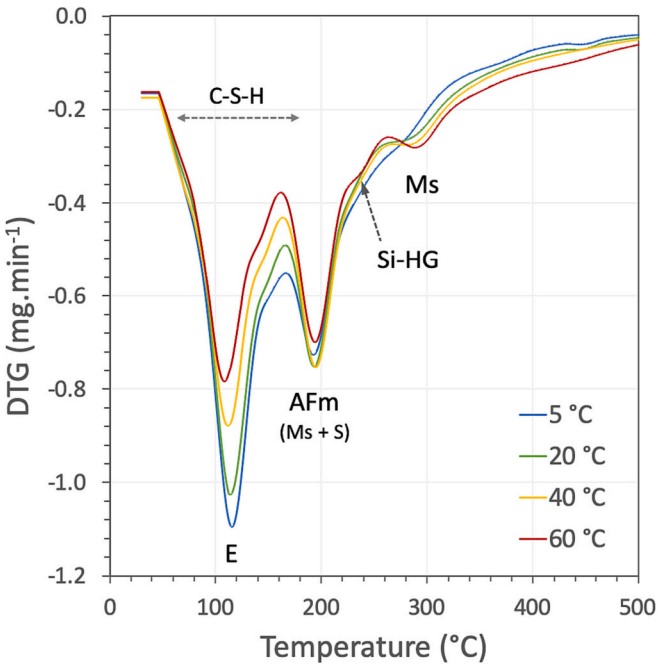

Fig. 11. Main hydration products at 180 days of hydration at all curing temperatures analysed by TGA curve: C-S-H = calcium silicate hydrates, E = ettringite, Ms = monosulfate, S = strätlingite, Si-HG = siliceous hydrogarnet.

3.3. Comparison of experimental data and thermodynamic modelling

At 28 days, ettringite, monosulfate and AH_3 are observed experimentally at all temperatures. A small amount of CAH_{10} and strätlingite are experimentally observed only at 5 °C. The amorphous content at 5 °C is higher than at the other temperatures. At 180 days, the main hydrates observed experimentally are ettringite, monosulfate, strätlingite and C-S-H at all temperatures. Siliceous hydrogarnet is observed only at 60 °C, as indicated by small broad XRD humps at ~17.5, 20.2 and 26.9° 2theta (see Appendix A). The occurrence of siliceous hydrogarnet only at 60 °C is related to a very low content of iron (< 0.1 %) in the BY cement, as the presence of iron favours the formation of siliceous hydrogarnet at room temperatures [52]. At very long reaction times (decades) monosulfate would be expected to transform to siliceous hydrogarnet (see Appendix B) as observed e.g. in 50 years old Portland cement [53]. However, AFm phases persist up to several years even though they are thermodynamically unstable. Fig. 6 shows the XRD patterns at 180 days of hydration at different temperatures focusing on the patterns between 28 and 34° (2theta), where the broad reflection typical for C-S-H [54] is expected. At the higher temperatures more belite has reacted, so more C-S-H is observed. In addition, the amounts of strätlingite and ettringite decrease, while more monosulfate is formed at higher temperature.

The measured reaction degrees of ye'elimite, anhydrite and belite at each time and temperature were used to predict the expected phases and quantities after 28 days and 180 days. The thermodynamic modelling is compared to the experimental assemblages determined by XRD-Rietveld and TGA in Fig. 7 (28 days) and Fig. 8 (180 days).

The experimental phase assemblages at 28 days are compared with the thermodynamic predictions in Fig. 6. Overall a good agreement is seen, particularly when the experimental errors are considered along with the poor crystallinity of the AFm phases, AH_3 and CAH_{10}. The amounts of ettringite found experimentally and predicted are in excellent agreement. The biggest discrepancy is observed for strätlingite, where thermodynamic modelling predicts quite large amounts at all temperatures, but none is seen experimentally apart from a trace at 5 °C. The absence of strätlingite reflections could be explained by its poor crystallinity and/or low quantity preventing detection by XRD. After

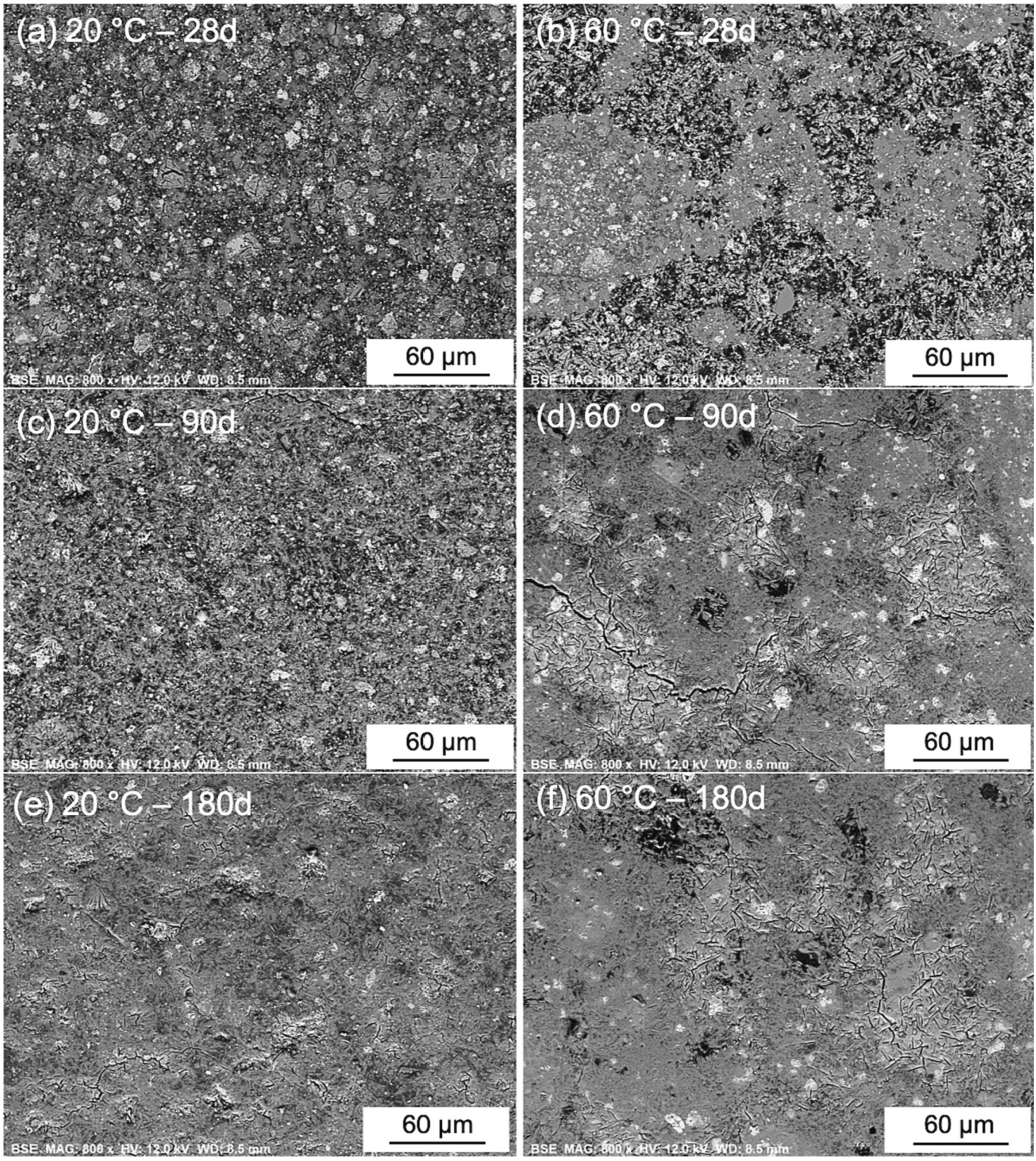

Fig. 12. Comparison of the general microstructures of BY cement cured at 20 and 60 °C at 28, 90 and 180 days.

180 days, more discrepancies with the experimental data are observed (Fig. 8) than after 28 days (Fig. 7). Experimentally, more ettringite and less monosulfate are observed than predicted by thermodynamic modelling. The amount of ettringite, detected by XRD-Rietveld is the lowest at 60 °C. This is consistent with the thermodynamic modelling prediction, although the predicted value is even lower, which might be related to the binding of sulfate in C-S-H. In addition, the Al-binding in C-S-H is not considered in thermodynamic modelling due to high interaction volume with other aluminate phases. Both experimental data and thermodynamic modelling show a similar trend of decreasing strätlingite content at elevated temperature although the amounts are significantly different. These discrepancies between the experimental and predicted phase assemblages are further investigated focusing on the influence of belite reaction.

The effect of belite reaction on the phase assemblages can be shown by thermodynamic modelling (Fig. 9). In the presence of AH_3, belite

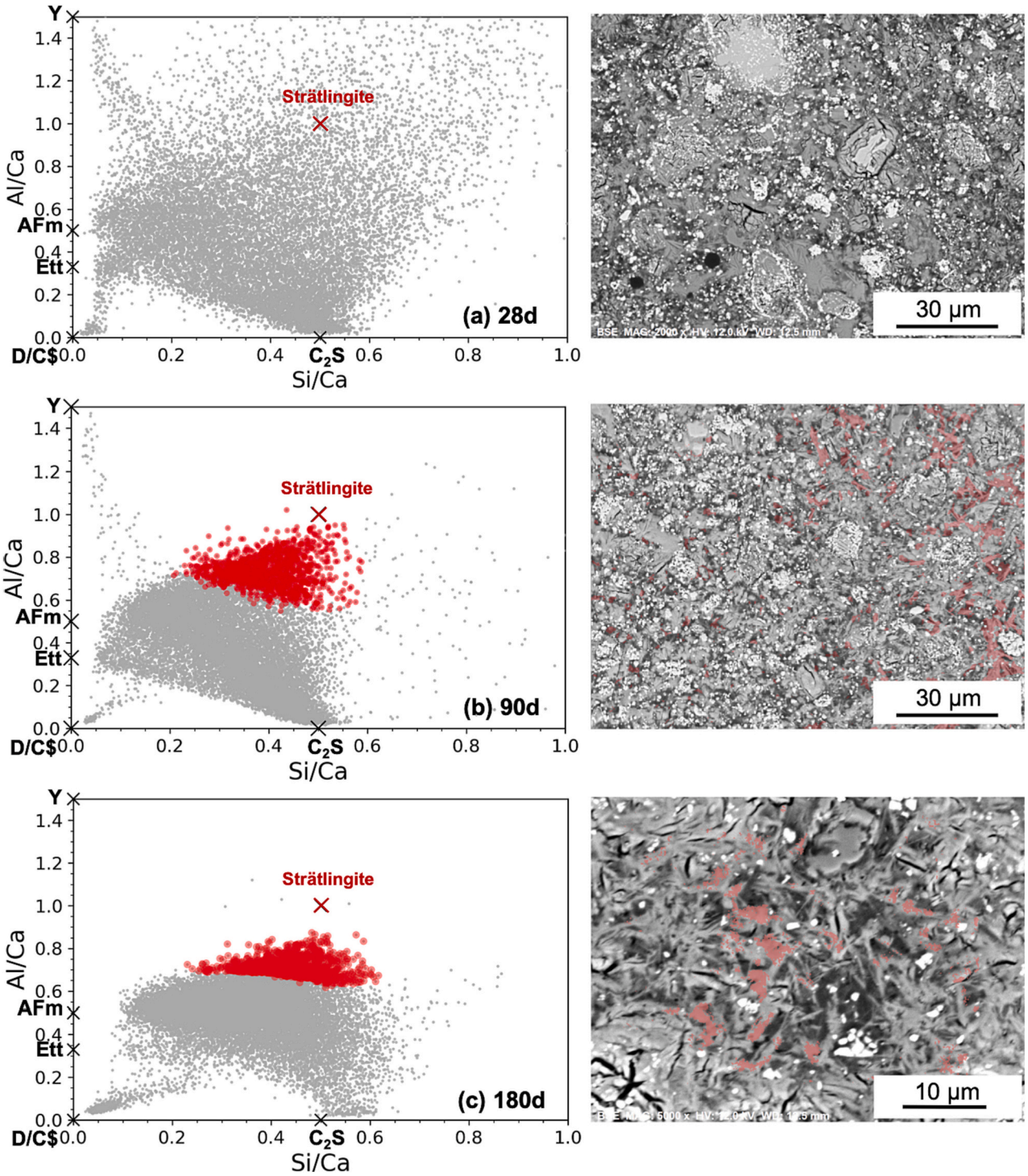

Fig. 13. The Si/Ca – Al/Ca ratio plots at (a) 28, (b) 90 and (c) 180 days showing strätlingite formation (red) in the microstructure cured at 20 °C: D = Dolomite, C$ = anhydrite, Ett = Ettringite, and Y = ye'elimite. (For interpretation of the references to colour in this figure legend, the reader is referred to the web version of this article.)

reacts to strätlingite (Eq. (3-1)). At high degree of belite reactions (> 40 % Fig. 9), AH_3 is no longer present. After this, the further reaction of belite destabilises strätlingite and ettringite to monosulfate and C-S-H (as illustrated by Eq. (3-2), C-S-H composition at 90 days, and Fig. 9). As a result, the amount of strätlingite and ettringite decrease with belite reaction and with time as also observed experimentally.

$$(\text{sufficient } AH_3): C_2S + AH_3 + 5H \rightarrow C_2ASH_8 \quad (3\text{-}1)$$

$$(\text{no more } AH_3): C_6A\bar{S}_3H_{32} + 6C_2S + 2C_2ASH_8 + 10H \rightarrow 3C_4A\bar{S}H_{14} + 8C_{1.25}SH_2 \quad (3\text{-}2)$$

In summary, the experimental data and thermodynamic modelling show reasonable qualitative agreement but there are differences in quantity for the AFm-type phases and ettringite, which might be due to a slow transformation of ettringite to AFm phases.

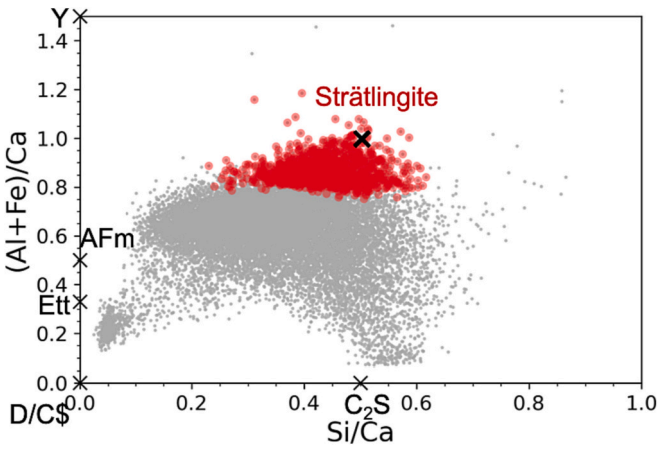

Fig. 14. The ratio plot of Si/Ca – (Al + Fe)/Ca of the microstructure at 180 days cured at 20 °C showing a possible Fe incorporation in strätlingite structure: D = Dolomite, C$ = anhydrite, Ett = Ettringite, and Y = ye'elimite.

3.4. AFm formation in BY cement

Thermodynamic modelling predicts more monosulfate and strätlingite than experimentally observed by XRD. Similar observations of more monosulfate predicted than observed have been reported previously for BYF cement [11]. The two main AFm phases forming in hydrated BY cement are monosulfate (Ms) and strätlingite (S), which both have a AFm-type layered structure with the general formula $[Ca_2Al(OH)_6]X{\cdot}yH_2O$, where X is the interlayer ions. AFm is often difficult to analyse quantitatively by XRD since the interlayer content can vary due to solid solution formation, which can result in broad XRD signals and an underestimation of the amount of AFm phases by XRD. In fact, Fig. 10, which illustrates the main reflections of hydrated BY cement between ~5° to 15° (2theta), shows the presence of two forms of monosulfate: Ms_{12} ($C_4A\bar{S}H_{12}$) and Ms_{14} ($C_2A\bar{S}H_{14}$), with different water contents [55]. The position of the Ms_{14} reflection at 2theta ~ 9.2° is close to the main reflection of ettringite (2theta ~ 9.0°), but clearly distinguishable, in particular at 60 °C. The Ms_{14} reflection is broader at lower temperature leading to more overlapping with the ettringite reflections. The overlapping peaks and the modified crystal structure lead to higher errors in quantification.

The XRD patterns in Fig. 10 confirm the precipitation of strätlingite at all temperatures in agreement with thermodynamic predictions. The formation of strätlingite at 60 °C in ettringite dominated systems has been reported recently [56]. The peaks of strätlingite at 40 and 60 °C are quite broad, indicating a poorly crystalline and asymmetric/internal disorder compared to the crystal structure used for the quantification [33]. The intensity of the characteristic peak of strätlingite around 7° 2theta is increased at lower temperature.

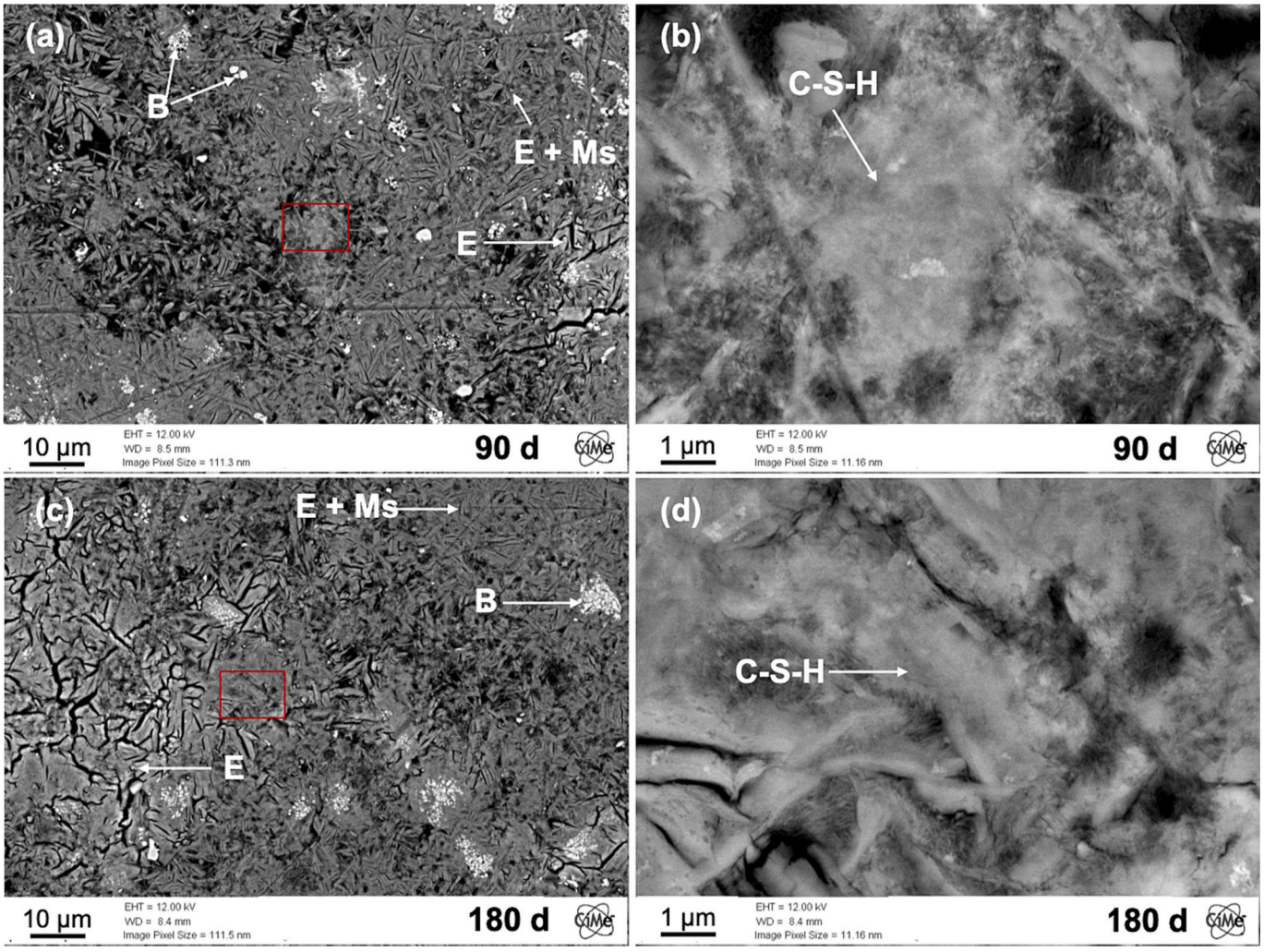

Fig. 15. Microstructure of C-S-H at (a, c) 90 and (b, d) 180 days cured at 60 °C with different magnification: B = Belite, E = Ettringite, Ms = Monosulfate, C-S-H = Calcium silicate hydrates.

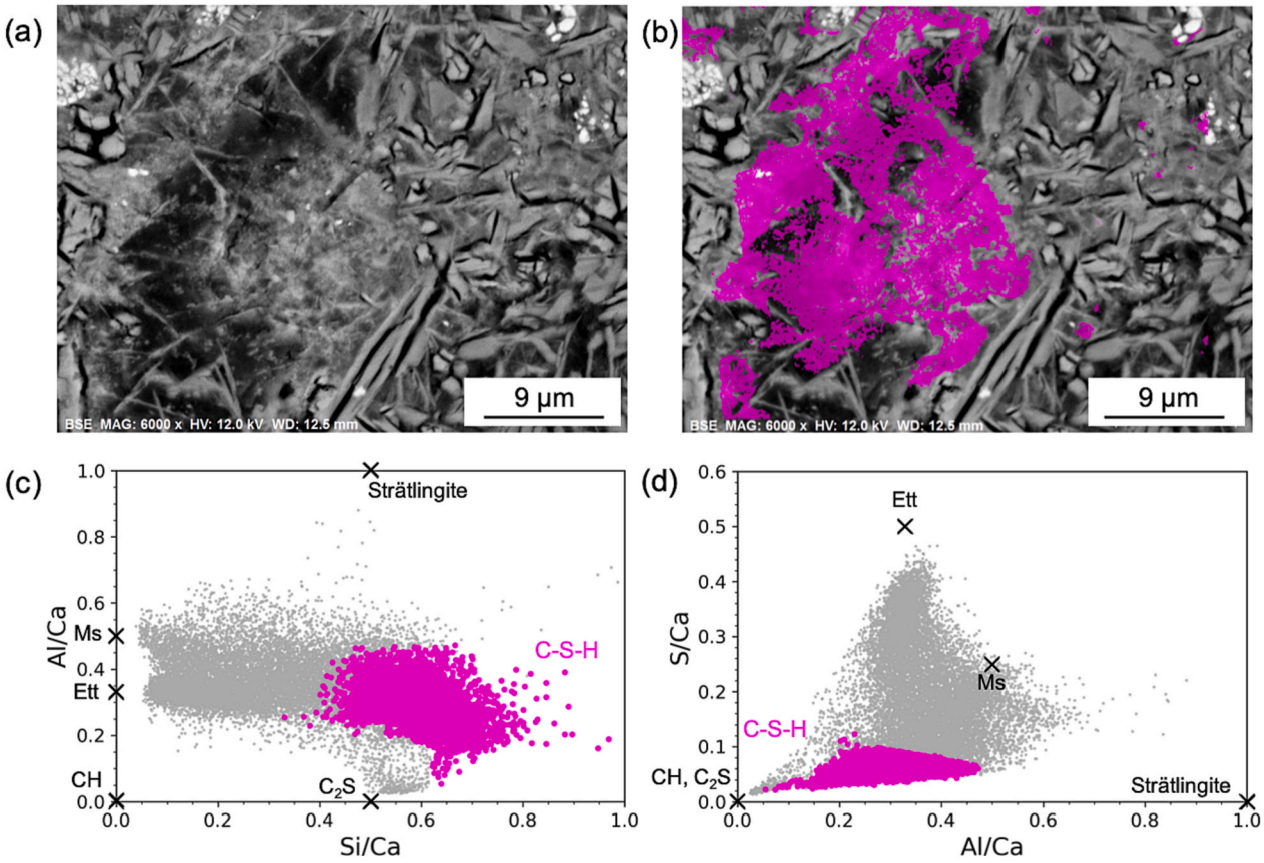

Fig. 16. Identification of C-S-H formation in BY cement at 90 days cured at 60 °C (a) BSE image (b) BSE image with C-S-H overlay as detected in (c) Si/Ca – Al/Ca ratio plot and (d) Al/Ca – S/Ca ratio plot. Ideal compositions of relevant phases are added to the ratio plots as guidelines: CH = Portlandite, Ett = Ettingite, Ms = Monosulfate, and C-S-H = calcium silicate hydrates.

Alternatively, AFm can be identified by TGA. The weight loss at around 200 °C in Fig. 11 is attributed to the dehydration of AFm-type phases [41], thus to monosulfate and strätlingite. The sample cured at 60 °C shows larger water loss peaks compared to the samples cured at 20 and 40 °C, indicating the presence of more AFm phases at 60 °C than quantified by XRD. The TGA data confirms that a significant amount of AFm phases are formed also at 5 and 60 °C, which are present as amorphous and/or microcrystalline phases and that the XRD data shown in Fig. 8 underestimate the amount of AFm phases present. The poor crystallinity might be related to higher disorder generated by a more pronounced solid solution formation or due to a formation of very small AFm grains/particles.

3.5. Microstructure of BY cement

The microstructure development of BY cement cured at 20 °C (low belite reaction), and 60 °C (high belite reaction) were investigated at 28, 90 and 180 days, as shown in Fig. 12. After 28 days of curing, the microstructure and porosity at 20 °C are more homogeneous than those of samples cured at 60 °C. At 90 days, the microstructure cured at 60 °C is less porous than 20 °C as belite reacts significantly (see Fig. 3) to C-S-H filling the pore space and at 180 days, a less porous microstructure is observed at both temperatures. Ettringite and monosulfate can be observed on the BSE images, but strätlingite and C-S-H are more difficult to find, particularly at low magnification. EDS mapping with image analysis was thus used to identify strätlingite and C-S-H in the microstructure of BY cement paste.

3.5.1. Strätlingite

The chemical composition of strätlingite in hydrated cement cannot be easily analysed by manual EDS point analysis as it is quite difficult to identify the strätlingite phase on a BSE image. Therefore, EDS mapping was carried out to identify strätlingite in the microstructure and estimate its composition. The ratio plots of Si/Ca and Al/Ca of the mappings are shown in Fig. 13.

The chemical composition of pure strätlingite is C_2ASH_8 corresponding to Si/Ca = 0.5 and Al/Ca = 1. The cloud of points observed after treatment EDS mapping lies between the composition of strätlingite and other AFm phases and ettringite, indicating intermixing as shown in Fig. 13. This figure shows the identification of strätlingite in the microstructure of BY at 20 °C by image analysis. The ratio plot of the microstructure at 28 days (Fig. 13a) shows a higher scatter of points compared to later ages. At this age, strätlingite is not detected by XRD (see Fig. 7) or EDS mapping. At 90 days, the EDS points close to the composition of strätlingite were manually selected in red; approximately Al/Ca > 0.6, Ca/Si = 0.2–0.6 to match the grains observed in the BSE image. Strätlingite in the hydrated BY cement is present as elongated grains, as shown in Fig. 13b, while it was difficult to specify the shape of strätlingite at 180 days as it is not present as separate grains. The microstructure at 180 days was investigated at a higher magnification to limit the area of the focus phase and minimize the intermixing of phases, by carefully choosing areas of interest based on the morphology of the hydrates. The ratio plot of Si/Ca and Al/Ca at 180 days (Fig. 13c) shows that the cloud of points is slightly shifted below the pure composition of strätlingite, compared to the sample at 90 days, indicating that some other elements, such as iron, could be present in the structure. The small amount of Fe originates from contamination in the natural anhydrite even though the Fe-containing phase has not been identified by XRD. Thus, the ratio plot of Si/Ca and (Al + Fe)/Ca at 180 days was plotted as shown in Fig. 14. In this view, the cloud of points reaches the

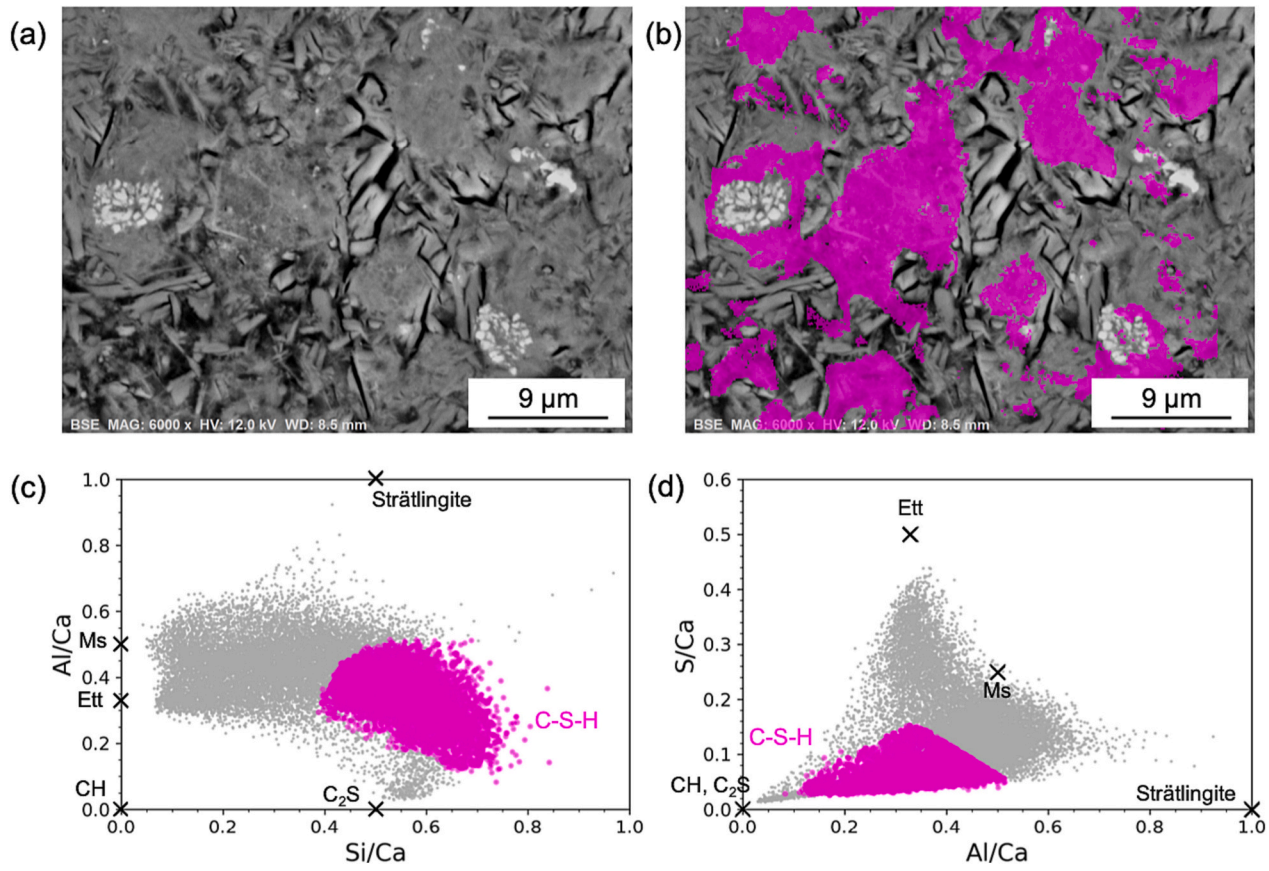

Fig. 17. Identification of C-S-H formation in BY cement at 180 days cured at 60 °C (a) BSE image (b) BSE image with C-S-H overlay as detected in (c) Si/Ca – Al/Ca ratio plot and (d) Al/Ca – S/Ca ratio plot: CH = Portlandite, Ett = Ettingite, Ms = Monosulfate, and C-S-H = calcium silicate hydrates.

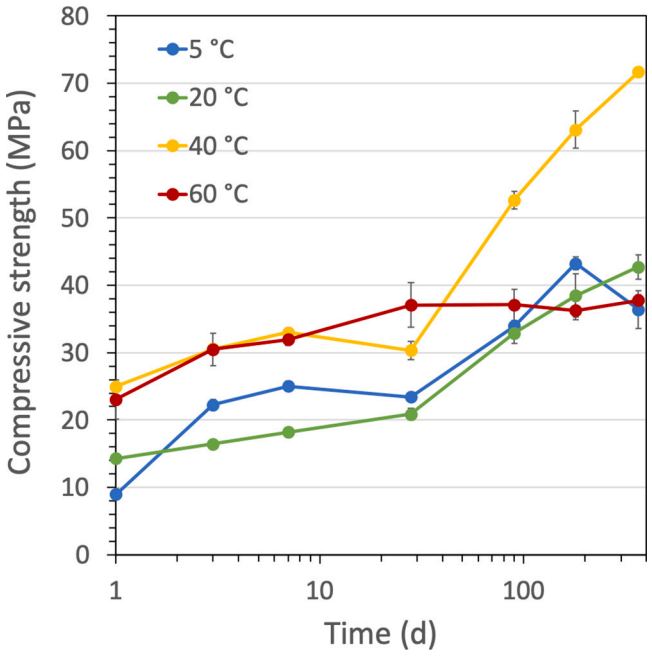

Fig. 18. Compressive strength development of BY system at different temperatures.

composition of strätlingite, indicating the presence of some Fe in the strätlingite structure. In Portland cement [53] and the samples at 60 °C with high belite reaction degree, Fe is present in siliceous hydrogarnet. In the low CaO belite-ye'elimite system at 20 °C no hydrogarnet is present resulting in the uptake of Fe in strätlingite, which is reported here for the first time.

The comparison of the chemical data with the EDS map indicates a fine distribution of strätlingite in the microstructure. The areas of strätlingite seem to be smaller than the interaction volume of the beam, such that they cannot be analysed as a separate phase. The higher AFm content predicted by thermodynamic modelling than observed experimentally by XRD seems to be related to their microcrystalline size, close intermixing with other phases and possibly variable interlayer composition. This limits the accuracy of XRD quantification, as also discussed in a previous study [12].

3.5.2. C-S-H

The formation of C-S-H in the microstructures cured at 60 °C at 90 and 180 days was also investigated by SEM. In contrast to the Portland cement system, where C-S-H generally grows from the surface of cement clinkers [57], no rim of inner C-S-H around belite grains was observed at 90 days (see Appendix D) At a low magnification of the BSE image in Fig. 15, C-S-H is quite difficult to detect due to its small size and its fine distribution between ettringite and monosulfate (present as platelets). At high magnification (Fig. 15b and d) C-S-H is visible.

EDS mapping and image analysis were used to further verify the presence of C-S-H. Figs. 16 and 17 show the BSE images of the region of interest, and the atomic ratio plots of Si/Ca-Al/Ca and Al/Ca-S/Ca from EDS mapping of BY cement cured at 60 °C at 90 and 180 days, respectively. The ratio plots of Si/Ca-Al/Ca in both samples (Figs. 16c and 17c) present a cloud of points towards high Si. The points with high Si content in the ratio plot were selected to identify the location of C-S-H, and displayed on the BSE image (using the edxia framework [42]). By comparison with Figs. 16b and 17b, it can be confirmed that the "fluffy"

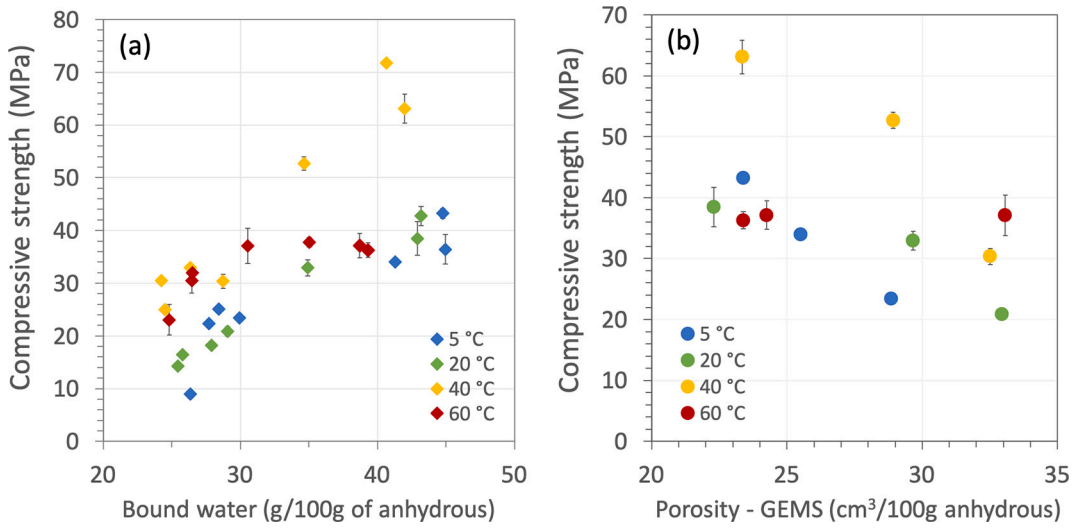

Fig. 19. The relationship between compressive strength cured at different temperatures and (a) bound water from 1 to 365 days characterized by TGA and (b) porosity calculated by thermodynamic modelling (GEMS) at 28, 90, and 180 days.

phase identified in Fig. 15 is indeed C-S-H. The C-S-H at 60 °C appears to have a high Al content in the ratio plots, consistent with the high Al-concentrations observed at 60 °C in the pore solution (see Fig. 2). Even though the EDS mapping is often used to characterise the chemical composition of C-S-H, it is difficult to analyse its composition in the BY cement due to its sparsity in the microstructure, and its fine intermixing with aluminate hydrates.

3.6. Compressive strength

The compressive strength was measured to put these microstructures in the more general context of common cementitious materials. The compressive strength of the BY system cured at different temperatures is shown in Fig. 18. There is no clear trend of compressive strength development as a function of temperature. Before 28 days, the strength slowly increases at all temperatures. A significant enhancement of compressive strength at a late age is correlated to the higher belite reaction (see Fig. 1) after 28 days, resulting in C-S-H formation filling the space. Although a high belite reaction is observed at 60 °C, the lack of a corresponding increase in compressive strength can be explained by the heterogeneous microstructure and the micro-cracks which can be observed on the mortar cube.

The relationships between compressive strength–bound water characterized by TGA, and compressive strength–porosity calculated from the difference between the initial volume and calculated volume of hydrates from thermodynamic modelling are shown in Fig. 19. The results of the sample cured at 60 °C are out of the trend due to micro-cracks and heterogenous microstructure, hence the data at 60 °C is not considered. An overall trend of the samples cured at different temperatures can be observed from both Fig. 19a and b. The trend of the samples cured at 5 and 20 °C are quite similar while the samples cured at 40 °C shows a significant development of compressive strength compared to bound water and porosity development. There is no clear explanation yet for the different trend at 40 °C than the other temperature. However, this seems to indicate that the precipitation of specific hydrates has more control over the macroscopic mechanical performances. In particular, the role of strätlingite and C-S-H precipitation need to be investigated further.

4. Conclusions

This study investigated the effect of temperature on phase assemblages and microstructure of a belite-ye'elimite cement. The comparison between experimental data and thermodynamic modelling and their discrepancies were carefully discussed. This revealed also that we lack knowledge of several aspects of the hydration of the belite-ye'elimite cements at various temperatures, in particular of:

1) Mechanisms limiting belite reaction at different temperature
2) C-S-H composition of BY cements
3) AFm crystallinity and stability
4) Fe substitution in strätlingite
5) Link between microstructure and performance

Ye'elimite reacts almost completely during the first day at all temperatures. In contrast, belite reacts very slowly during the first 28 days of hydration. When the reaction of belite starts, AH_3 and CAH_{10} disappear from the hydrate assemblage, which occurs only after 90 days at 20 and 40 °C, but earlier at 5 and 60 °C, leading to differences in the phase assemblages with the temperature at 90 days. After 180 and 365 days, more belite reaction is observed at a higher temperature. The mechanisms that govern the reaction of belite in the CSA are unclear.

At high ye'elimite reaction and low belite reaction degrees (i.e. up to 28 days), the formation of mainly monosulfate, ettringite and AH_3 is observed together with some strätlingite. At 5 °C, CAH_{10} instead of AH_3 is present. After 180 days and longer, when most of the belite has reacted, AH_3 disappears and the formation of C-S-H is observed. The comparison of the experimental data with thermodynamic modelling shows an overall reasonable agreement. Some discrepancies were observed in the quantities of hydrated phases. Higher amounts of AFm phases, monosulfate and strätlingite, are predicted compared to the experimental observation, which can be explained by the formation of poorly or microcrystalline of AFm phases which are only partially captured in an XRD quantification. At 180 days, somewhat more monosulfate and C-S-H, and less strätlingite and ettringite, are observed at a higher temperature where more belite had reacted.

The strätlingite is finely intermixed with monosulfate and is present as elongated grains at 20 °C. SEM/EDS mapping indicates lower Al content in strätlingite structure than expected, possibly due to the presence of Fe content in its structure.

C-S-H is formed when the degree of reaction of belite is high (> 50 %). Although XRD Rietveld cannot quantify the amount of C-S-H due to its amorphous form, the formation of C-S-H was confirmed by XRD, and SEM-EDS at 90 days and longer. C-S-H is formed finely intermixed with other aluminate hydrates such that its composition cannot be estimated accurately.

Curing at high temperatures tends to give higher strength at an early age. Finally, the late reaction of belite leads to additional strength. A general correlation was found between compressive strength and bound water or porosity. However, the temperature effect on this correlation is still unclear. Further investigation on the morphology of hydrates precipitation is needed after belite reaction, particularly for the C-S-H and strätlingite phases and their morphology.

CRediT authorship contribution statement

Natechanok Chitvoranund: Methodology, Formal analysis, Investigation, Writing – original draft, Visualization. **Barbara Lothenbach:** Conceptualization, Methodology, Formal analysis, Writing – review & editing, Supervision, Funding acquisition. **Diana Londono Zuluaga:** Methodology, Writing – review & editing. **Frank Winnefeld:** Supervision, Writing – review & editing. **Karen Scrivener:** Conceptualization, Supervision, Writing – review & editing, Funding acquisition.

Declaration of competing interest

The authors declare that they have no known competing financial interests or personal relationships that could have appeared to influence the work reported in this paper.

Data availability

Data will be made available on request.

Acknowledgement

This work was financially supported by Nanocem, a consortium of academic and industrial partners for cement and concrete research as part of the Core Project 16. The author would like to acknowledge Josef Kaufmann for the particle size distribution discussion, Mohsen Ben Haha, Frank Bullerjahn, Arnaud Muller, Xuerun Li and Duncan Herfort for the help with clinker preparation, Beat Münch for SEM/EDS method, Fabien Georget for image analysis and discussions, Mahsa Bagheri for high resolution scanning electron microscope, and Andrea Teixeira for XRD results.

Appendix A

The XRD patterns of BY cement after 28, 180 and 365 days of hydration at different temperatures are shown in Figs. 20, 21, and 22, respectively. The presence of Hc and Mc in the sample cured at 20 °C is probably due to the sample was carbonated during curing.

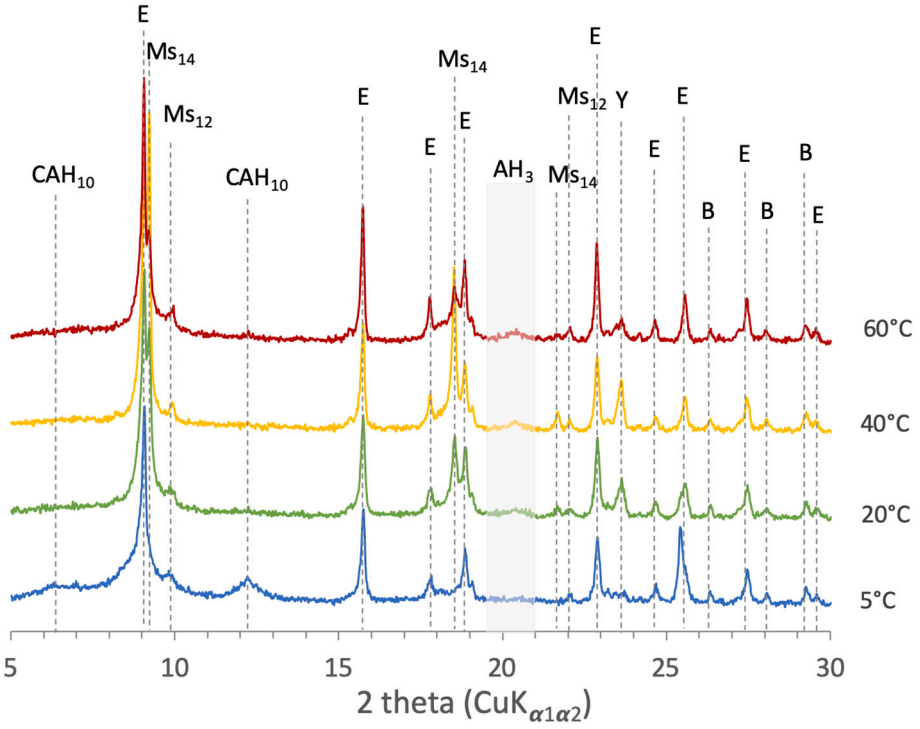

Fig. 20. XRD patterns of BY cement after 28 days of hydration cured at 5, 20, 40 and 60 °C at the zoom section between 5 and 30° 2theta: B = belite, Y = ye'limite, E = ettringite, Ms = monosulfate.

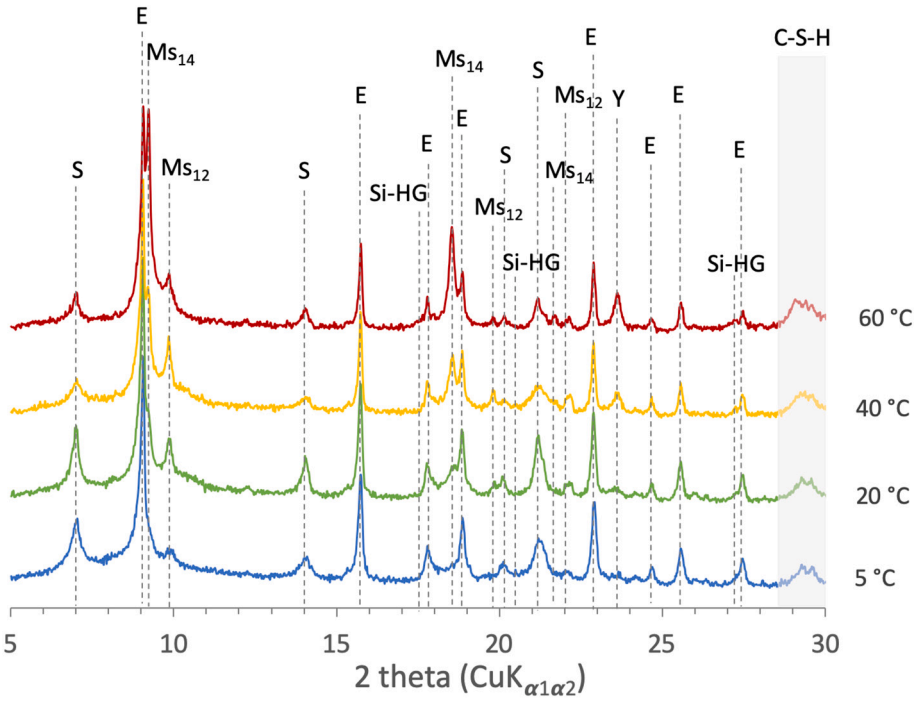

Fig. 21. XRD patterns of BY cement after 180 days of hydration cured at 5, 20, 40 and 60 °C at the zoom section between 5 and 30° 2theta: Y = ye'limite, E = ettringite, Ms = monosulfate, S = strätlingite, Si-HG = silicious hydrogarnet, C-S-H = calcium silicate hydrates.

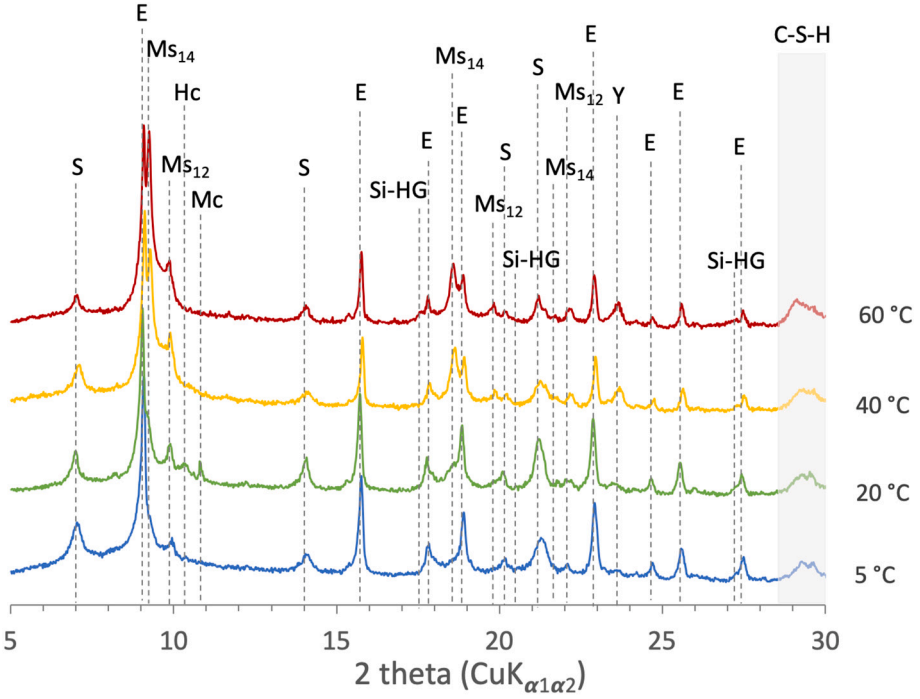

Fig. 22. XRD patterns of BY cement after 365 days of hydration cured at 5, 20, 40 and 60 °C at the zoom section between 5 and 30° 2theta: Y = ye'limite, E = ettringite, Hc = hemicarbonate, Mc = monocarbonate, Ms = monosulfate, S = strätlingite, Si-HG = silicious hydrogarnet, C-S-H = calcium silicate hydrates.

Appendix B

The pore solution at 90 days and the calculation of the effective saturation index of BY cement at 90 days cured at 5, 20, 40 and 60 °C are shown in Tables 4 and 5 respectively.

Table 4
Ion concentrations in the pore solution of BY cement at 90 days cured at different temperatures.

	5 °C	20 °C	40 °C	60 °C
Na (mmol/l)	37	33	27	32
K (mmol/l)	0.6	0.8	0.2	0.2
Ca (mmol/l)	7.1	1.1	0.8	0.8
Cl (mmol/l)	0.7	4.7	4.8	5.0
SO_4 (mmol/l)	0.1	3.2	1.7	3.4
Si (mmol/l)	0.02	0.14	0.10	0.09
Al (mmol/l)	0.1	5.0	4.5	6.2
OH^- (mmol/l)	51	19	16	15

Table 5
Effective saturation index (SI) calculated from ion concentration of BY cement pore solution at 90 days cured at different temperatures.

Effective SI	5 °C	20 °C	40 °C	60 °C
Belite	−0.6	−0.7	−0.6	−0.5
Anhydrite	−1.4	−1.0	−1.1	−0.8
Ettringite	0.3	0.3	0.0	−0.1
Monosulfate	0.1	0.1	−0.1	−0.1
$Al(OH)_{3mic}$	−1.2	0.0	−0.1	0.0
CAH_{10}	−1.1	−0.2	−0.6	−0.6
Strätlingite	−0.2	0.4	0.1	0.1
C-S-H	−0.1	−0.1	−0.1	−0.1

Appendix C

Siliceous hydrogarnet is observed at 60 °C in the experimental data. In the modelling, generally only the formation of mixed Al—Fe containing hydrogarnets is allowed as such Al-Fe-containing siliceous hydrogarnet ($C_3(AF)S_{0.84}H$) form readily also at ambient temperature [53]. As no significant amount of iron is present in the studied BY cement ($Fe_2O_3 < 0.1$ %), also no siliceous hydrogarnet has been predicted.

Aluminium containing siliceous hydrogarnet are usually observed at high temperatures only [16,17,58], as a solid solution between katoite (C_3AH_6, $Ca_3Al_2(OH)_{12}$) and grossularite (C_3AS_3, $C_3Al_2Si_3O_{12}$). Their formation is generally prevented at ambient temperature in thermodynamic modelling, due to their slow kinetics of formation [52,59], although aluminium containing siliceous hydrogarnet would be thermodynamically more stable than AFm phases. As the formation of siliceous hydrogarnet is faster at high temperature, the formation of aluminium-based siliceous hydrogarnet was allowed in the thermodynamic modelling calculation at 60 °C.

Fig. 23 shows a comparison between the experimental data at 60 °C and thermodynamic modelling based on three different assumptions: i) without, ii) with a restricted amount and iii) with free formation of aluminium based-siliceous hydrogarnet. If the formation of siliceous hydrogarnet is not constrained, a large amount of aluminium-based siliceous hydrogarnet forms as a stable phase while monosulfate and strätlingite are destabilised, and ettringite content is significantly increased. The comparison of the experimental data with the different modelling results indicates that the phase assemblages at 180 days at 60 °C is not yet at equilibrium; the observed phase assemblage corresponds best to the intermediate case were only a limited amount of aluminium-based siliceous hydrogarnet is considered. Even under these conditions, the amount of monosulfate and strätlingite is higher than the experimental observation.

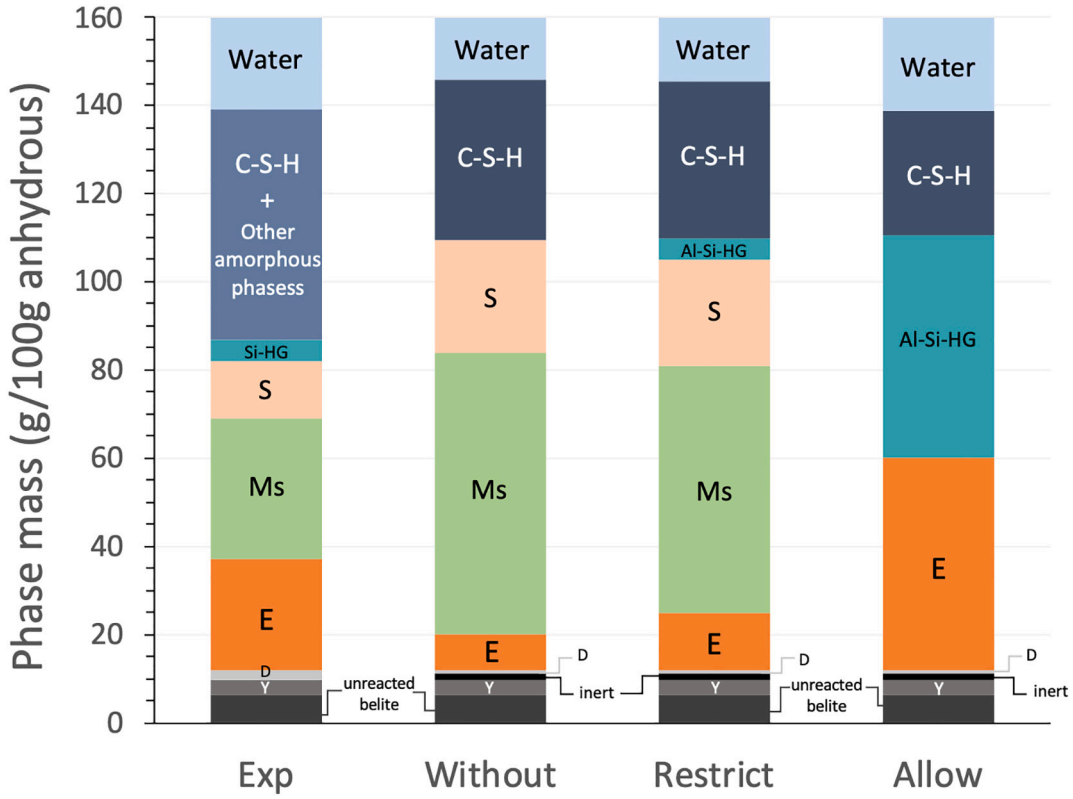

Fig. 23. Thermodynamic modelling calculations: without Al-containing siliceous hydrogarnet (Al-Si-HG), a restricted amount of Al-Si-HG and freely allowed Al-Si-HG at 60 °C compared to experimental data: Y = ye'limite, D = Dolomite, E = ettringite, Ms = monosulfate, S = strätlingite, Si-HG = silicious hydrogarnet, C-S-H = calcium silicate hydrates.

Appendix D

The formation of C-S-H in the microstructures cured at 60 °C at 90 and 180 days showing no rim of inner C-S-H around belite grains was observed at 90 days.

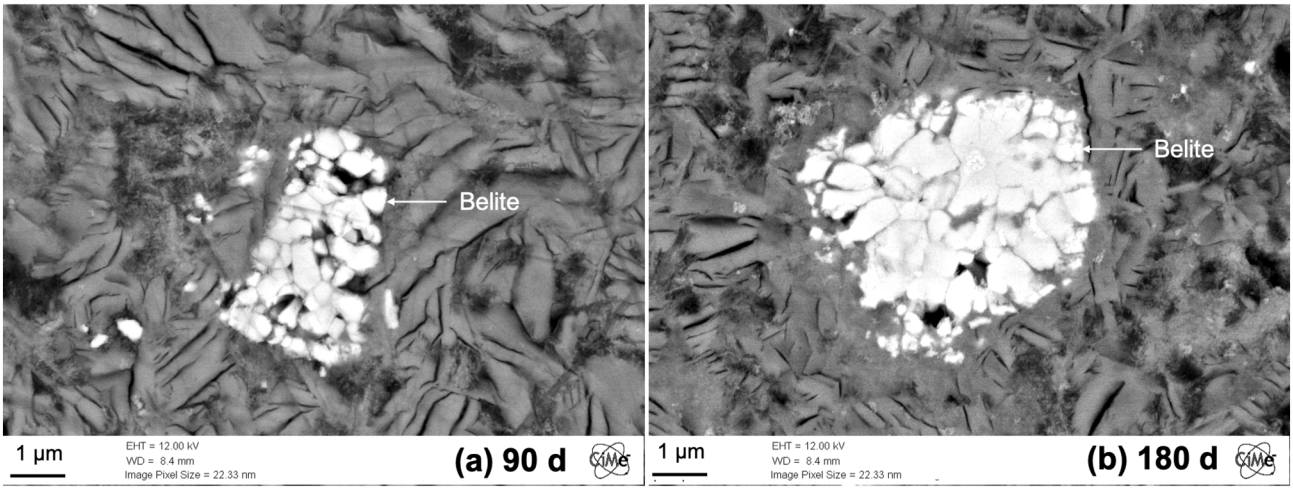

Fig. 24. Microstructure around belite grains cured 60 °C at (a) 90 and (b) 180 days with high-resolution SEM.

References

[1] E. Gartner, Industrially interesting approaches to "low-CO2" cements, Cem. Concr. Res. 34 (2004) 1489–1498, https://doi.org/10.1016/j.cemconres.2004.01.021.
[2] E. Gartner, H. Hirao, A review of alternative approaches to the reduction of CO2 emissions associated with the manufacture of the binder phase in concrete, Cem. Concr. Res. 78 (2015) 126–142, https://doi.org/10.1016/j.cemconres.2015.04.012.
[3] F. Winnefeld, B. Lothenbach, Hydration of calcium sulfoaluminate cements — experimental findings and thermodynamic modelling, Cem. Concr. Res. 40 (2010) 1239–1247, https://doi.org/10.1016/j.cemconres.2009.08.014.

[4] D. Londono-Zuluaga, J.I. Tobón, M.A.G. Aranda, I. Santacruz, A.G. De la Torre, Clinkering and hydration of belite-alite-ye'elimite cement, Cem. Concr. Compos. 80 (2017) 333–341, https://doi.org/10.1016/j.cemconcomp.2017.04.002.

[5] K. Quillin, Performance of belite–sulfoaluminate cements, Cem. Concr. Res. 31 (2001) 1341–1349, https://doi.org/10.1016/S0008-8846(01)00543-9.

[6] J.J. Wolf, Application of thermodynamic modeling to predict the stable hydrate phase assemblages in ternary CSA-OPC-anhydrite systems and quantitative verification by QXRD, Cem. Concr. Res. 9 (2020).

[7] F. Winnefeld, B. Lothenbach, Phase equilibria in the system Ca4Al6O12SO4 – Ca2SiO4 – CaSO4 – H2O referring to the hydration of calcium sulfoaluminate cements, RILEM Tech. Lett. 7 (2016).

[8] F. Song, Z. Yu, F. Yang, Y. Lu, Y. Liu, Microstructure of amorphous aluminum hydroxide in belite-calcium sulfoaluminate cement, Cem. Concr. Res. 71 (2015) 1–6, https://doi.org/10.1016/j.cemconres.2015.01.013.

[9] C.W. Hargis, B. Lothenbach, C.J. Müller, F. Winnefeld, Further insights into calcium sulfoaluminate cement expansion, Adv. Cem. Res. 31 (2019) 160–177, https://doi.org/10.1680/jadcr.18.00124.

[10] F. Winnefeld, B. Lothenbach, On the Occurrence of CAH10 in Hydrated Calcium Sulfoaluminate Cements, in: SP-349 11th ACIRILEM Int. Conf. Cem. Mater. Altern. Bind. Sustain. Concr, American Concrete Institute, 2021, https://doi.org/10.14359/51732744.

[11] V. Morin, P. Termkhajornkit, B. Huet, G. Pham, Impact of quantity of anhydrite, water to binder ratio, fineness on kinetics and phase assemblage of belite-ye'elimite-ferrite cement, Cem. Concr. Res. 99 (2017) 8–17, https://doi.org/10.1016/j.cemconres.2017.04.014.

[12] M. Zajac, J. Skocek, C. Stabler, F. Bullerjahn, M. Ben Haha, Hydration and performance evolution of belite–ye'elimite–ferrite cement, Adv. Cem. Res. 31 (2019) 124–137, https://doi.org/10.1680/jadcr.18.00110.

[13] J. Wang, Hydration Mechanism of Cements Based on Low-CO2 Clinkers Containing Belite, ye'elimite and Calcium Alumino-Ferrite, n.d.

[14] G. Álvarez-Pinazo, I. Santacruz, M.A.G. Aranda, Hydration of belite–ye'elimite–ferrite cements with different calcium sulfate sources, Adv. Cem. Res. 28 (2016) 529–543, https://doi.org/10.1680/jadcr.16.00030.

[15] F. Bullerjahn, M. Zajac, M. Ben Haha, K.L. Scrivener, Factors influencing the hydration kinetics of ye'elimite; effect of mayenite, Cem. Concr. Res. 116 (2019) 113–119, https://doi.org/10.1016/j.cemconres.2018.10.026.

[16] P. Wang, N. Li, L. Xu, Hydration evolution and compressive strength of calcium sulphoaluminate cement constantly cured over the temperature range of 0 to 80 °C, Cem. Concr. Res. 100 (2017) 203–213, https://doi.org/10.1016/j.cemconres.2017.05.025.

[17] J. Kaufmann, F. Winnefeld, B. Lothenbach, Stability of ettringite in CSA cement at elevated temperatures, Adv. Cem. Res. 28 (2016) 251–261, https://doi.org/10.1680/jadcr.15.00029.

[18] E. Gartner, T. Sui, Alternative cement clinkers, Cem. Concr. Res. 114 (2018) 27–39, https://doi.org/10.1016/j.cemconres.2017.02.002.

[19] R.B. Perkins, C.D. Palmer, Solubility of ettringite (Ca6[Al(OH)6]2(SO4)3 · 26H2O) at 5–75°C, Geochim. Cosmochim. Acta 63 (1999) 1969–1980, https://doi.org/10.1016/S0016-7037(99)00078-2.

[20] B. Lothenbach, D.A. Kulik, T. Matschei, M. Balonis, L. Baquerizo, B. Dilnesa, G. D. Miron, R.J. Myers, Cemdata18: a chemical thermodynamic database for hydrated Portland cements and alkali-activated materials, Cem. Concr. Res. 115 (2019) 472–506, https://doi.org/10.1016/j.cemconres.2018.04.018.

[21] L.H.J. Martin, F. Winnefeld, E. Tschopp, C.J. Müller, B. Lothenbach, Influence of fly ash on the hydration of calcium sulfoaluminate cement, Cem. Concr. Res. 12 (2017).

[22] D. Jansen, J.J. Wolf, N. Fobbe, The hydration of nearly pure ye'elimite with a sulfate carrier in a stoichiometric ettringite binder system. Implications for the hydration process based on in-situ XRD, 1H-TD-NMR, pore solution analysis, and thermodynamic modeling, Cem. Concr. Res. 127 (2020) 105923. doi:https://doi.org/10.1016/j.cemconres.2019.105923.

[23] C.W. Hargis, B. Lothenbach, C.J. Müller, F. Winnefeld, Carbonation of calcium sulfoaluminate mortars, Cem. Concr. Compos. 80 (2017) 123–134, https://doi.org/10.1016/j.cemconcomp.2017.03.003.

[24] X. Li, A. Ouzia, K. Scrivener, Laboratory synthesis of C3S on the kilogram scale, Cem. Concr. Res. 108 (2018) 201–207, https://doi.org/10.1016/j.cemconres.2018.03.019.

[25] D. Jansen, F. Goetz-Neunhoeffer, B. Lothenbach, J. Neubauer, The early hydration of Ordinary Portland Cement (OPC): an approach comparing measured heat flow with calculated heat flow from QXRD, Cem. Concr. Res. 42 (2012) 134–138, https://doi.org/10.1016/j.cemconres.2011.09.001.

[26] S.T. Bergold, F. Goetz-Neunhoeffer, J. Neubauer, Quantitative analysis of C–S–H in hydrating alite pastes by in-situ XRD, Cem. Concr. Res. 53 (2013) 119–126, https://doi.org/10.1016/j.cemconres.2013.06.001.

[27] R. Allmann, Refinement of the hybrid layer structure [Ca2Al(OH)6]+·[1/2SO4·3H2O], Neues Jahrb. Mineral. Monatshefte (1977) 136–144.

[28] W.G. Mumme, R.J. Hill, G. Bushnell-Wye, E.R. Segnit, Rietveld crystal structure refinements, crystal chemistry and calculated powder diffraction data for the polymorphs of dicalcium silicate and related phases, Neues Jahrb. Fuer Mineral. - Abh. 169 (1995) 35–68.

[29] F. Guirado, S. Galí, S. Chinchón, J. Rius, Crystal structure solution of hydrated high-alumina cemetn from X-ray powder diffraction data**, Angew. Chem. 37 (1998) 72–75, https://doi.org/10.1002/(SICI)1521-3773(19980202)37:1/2<72::AID-ANIE72>3.0.CO;2-8.

[30] N.J. Calos, C.H.L. Kennard, A.K. Whittaker, R.L. Davis, Structure of Calcium Aluminate Sulfate Ca4Al6O16S, J. Solid State Chem. 119 (1995) 1–7.

[31] H. Saalfeld, Refinement of the crystal structure of gibbsite, AI(OH)3, Z. Für Krist. Krist. Krstallphysik Krist. 139 (1974) 129–135.

[32] H. Saalfeld, W. Depmeier, Silicon-free compounds with sodalite structure, Krist. Tech. 7 (1972) 229–233, https://doi.org/10.1002/crat.19720070125.

[33] R. Rinaldi, M. Sacerdoti, E. Passaglia, Strätlingite: crystal structure, chemistry, and a reexamination of its polytpye vertumnite, Eur. J. Mineral. 2 (1990) 841–850.

[34] V.I. Ponomarev, D.M. Kheiker, N.V. Belov, Crystal structure of tetracalcium trialuminate - the aluminate analog of sodalite, Kristallografija 15 (1970) 918–921.

[35] F. Goetz-Neunhoeffer, J. Neubauer, Refined ettringite (Ca6Al2(SO4)3(OH)12•26H2O) structure for quantitative X-ray diffraction analysis, Powder Diffract. 21 (2006) 4–11, https://doi.org/10.1154/1.2146207.

[36] J.C.A. Boeyens, V.V.H. Ichharam, Redetermination of the crystal structure of calcium sulphate dihydrate, Z. Für Krist. - New Cryst. Struct. 217 (2002) 9–10.

[37] E. Höhne, A more accurate determination of the crystal structure of anhydrite, CaSO4, Sov. Phys.-Crystallogr. 7 (1963) 559–569.

[38] N.L. Ross, R.J. Reeder, High-pressure structural study of dolomite and ankerite, Am. Mineral. 77 (1992) 412–421.

[39] O. Ferro, E. Galli, G. Papp, S. Quartieri, S. Szakall, G. Vezzalini, A new occurrence of Katoite and re-examination of the hydrogrossular group, Eur. J. Mineral. 15 (2003) 419–426.

[40] I.G. Richardson, Model structures for C-(a)-S-H(I), Acta Crystallogr. Sect. B Struct. Sci. Cryst. Eng. Mater. 70 (2014) 903–923, https://doi.org/10.1107/S2052520614021982.

[41] K. Scrivener, R. Snellings, B. Lothenbach (Eds.), A Practical Guide to Microstructural Analysis of Cementitious Materials, CRC Press, Boca Raton, 2016.

[42] F. Georget, W. Wilson, K.L. Scrivener, edxia: Microstructure characterisation from quantified SEM-EDS hypermaps, Cem. Concr. Res. 141 (2021) 106327, https://doi.org/10.1016/j.cemconres.2020.106327.

[43] R.S. Barneyback, S. Diamond, Expression and analysis of pore fluids from hardened cement pastes and mortars, Cem. Concr. Res. 11 (1981) 279–285, https://doi.org/10.1016/0008-8846(81)90069-7.

[44] B. Traynor, H. Uvegi, E. Olivetti, B. Lothenbach, R.J. Myers, Methodology for pH measurement in high alkali cementitious systems, Cem. Concr. Res. 135 (2020) 106122, https://doi.org/10.1016/j.cemconres.2020.106122.

[45] D.A. Kulik, T. Wagner, S.V. Dmytrieva, G. Kosakowski, F.F. Hingerl, K. V. Chudnenko, U.R. Berner, GEM-Selektor geochemical modeling package: revised algorithm and GEMS3K numerical kernel for coupled simulation codes, Comput. Geosci. (2012), https://doi.org/10.1007/s10596-012-9310-6.

[46] T. Wagner, D.A. Kulik, F.F. Hingerl, S.V. Dmytrieva, GEM-Selektor geochemical modeling package: TSolMod library and data interface for multicomponent phase models, Can. Mineral. 50 (2012) 1173–1195, https://doi.org/10.3749/canmin.50.5.1173.

[47] W. Hummel, U. Berner, E. Curti, F.J. Pearson, T. Thoenen, Nagra/PSI chemical thermodynamic data base 01/01, Radiochim. Acta. 90 (2002), https://doi.org/10.1524/ract.2002.90.9-11_2002.805.

[48] L. Nicoleau, E. Schreiner, A. Nonat, Ion-specific effects influencing the dissolution of tricalcium silicate, Cem. Concr. Res. 59 (2014) 118–138, https://doi.org/10.1016/j.cemconres.2014.02.006.

[49] E. Pustovgar, R.K. Mishra, M. Palacios, J.-B. d'Espinose de Lacaillerie, T. Matschei, A.S. Andreev, H. Heinz, R. Verel, R.J. Flatt, Influence of aluminates on the hydration kinetics of tricalcium silicate, Cem. Concr. Res. 100 (2017) 245–262, https://doi.org/10.1016/j.cemconres.2017.06.006.

[50] B. Lothenbach, L. Pelletier-Chaignat, F. Winnefeld, Stability in the system CaO–Al2O3–H2O, Cem. Concr. Res. 42 (2012) 1621–1634, https://doi.org/10.1016/j.cemconres.2012.09.002.

[51] L.G. Baquerizo, T. Matschei, K.L. Scrivener, M. Saeidpour, L. Wadsö, Hydration states of AFm cement phases, Cem. Concr. Res. 73 (2015) 143–157, https://doi.org/10.1016/j.cemconres.2015.02.011.

[52] B.Z. Dilnesa, B. Lothenbach, G. Renaudin, A. Wichser, D. Kulik, Synthesis and characterization of hydrogarnet Ca3(AlxFe1−x)2(SiO4)y(OH)4(3−y), Cem. Concr. Res. 59 (2014) 96–111, https://doi.org/10.1016/j.cemconres.2014.02.001.

[53] B.Z. Dilnesa, E. Wieland, B. Lothenbach, R. Dähn, K.L. Scrivener, Fe-containing phases in hydrated cements, Cem. Concr. Res. 58 (2014) 45–55, https://doi.org/10.1016/j.cemconres.2013.12.012.

[54] E. L'Hôpital, B. Lothenbach, D.A. Kulik, K. Scrivener, Influence of calcium to silica ratio on aluminium uptake in calcium silicate hydrate, Cem. Concr. Res. 85 (2016) 111–121, https://doi.org/10.1016/j.cemconres.2016.01.014.

[55] L.G. Baquerizo, T. Matschei, K.L. Scrivener, M. Saeidpour, A. Thorell, L. Wadsö, Methods to determine hydration states of minerals and cement hydrates, Cem. Concr. Res. 65 (2014) 85–95, https://doi.org/10.1016/j.cemconres.2014.07.009.

[56] H. Nguyen, V. Carvelli, W. Kunther, M. Illikainen, P. Kinnunen, Phase evolution and mechanical performance of an ettringite-based binder during hydrothermal aging, Cem. Concr. Res. 143 (2021) 106403, https://doi.org/10.1016/j.cemconres.2021.106403.

[57] J.E. Rossen, K.L. Scrivener, Optimization of SEM-EDS to determine the C–A–S–H composition in matured cement paste samples, Mater Charact 123 (2017) 294–306, https://doi.org/10.1016/j.matchar.2016.11.041.

[58] M. Paul, F.P. Glasser, Impact of prolonged warm (85°C) moist cure on Portland cement paste, Cem. Concr. Res. 30 (2000) 1869–1877, https://doi.org/10.1016/S0008-8846(00)00286-6.

[59] B. Lothenbach, T. Matschei, G. Möschner, F.P. Glasser, Thermodynamic modelling of the effect of temperature on the hydration and porosity of Portland cement, Cem. Concr. Res. 38 (2008) 1–18, https://doi.org/10.1016/j.cemconres.2007.08.017.